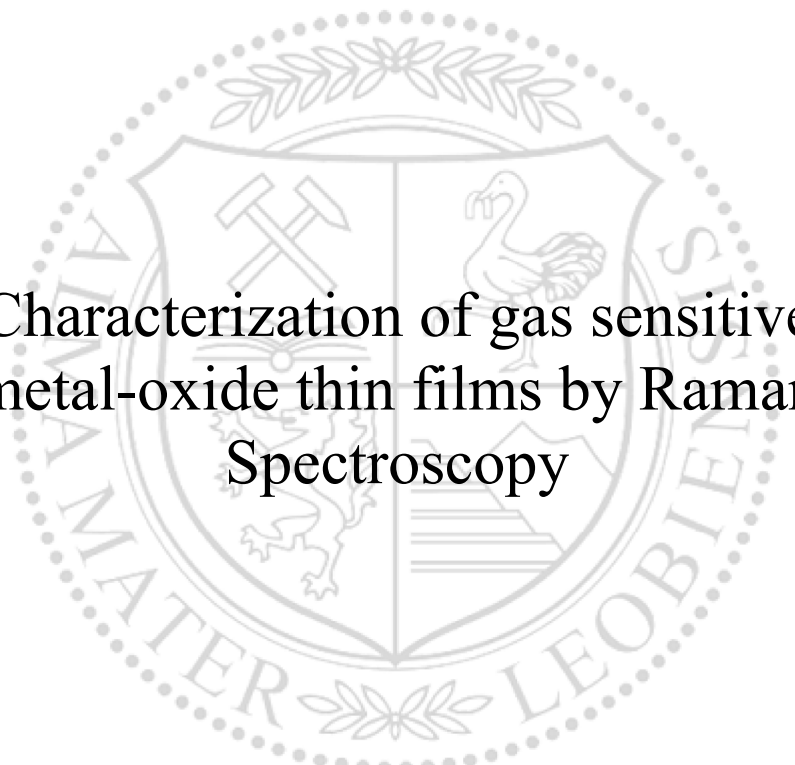




Chair of Functional Materials and Materials Systems

Master's Thesis

The background features a large, faint watermark of the University of Leoben seal. The seal is circular and contains a shield with various symbols: a hammer and pickaxe, a swan, and a lion. The text 'UNIVERSITAS MONTANA LEOBENSIS' is visible around the perimeter of the seal.

Characterization of gas sensitive
metal-oxide thin films by Raman
Spectroscopy

Marco Sebastian Holzer, BSc

November 2019

EIDESSTÄTTLICHE ERKLÄRUNG

Ich erkläre an Eides statt, dass ich diese Arbeit selbständig verfasst, andere als die angegebenen Quellen und Hilfsmittel nicht benutzt, und mich auch sonst keiner unerlaubten Hilfsmittel bedient habe.

Ich erkläre, dass ich die Richtlinien des Senats der Montanuniversität Leoben zu "Gute wissenschaftliche Praxis" gelesen, verstanden und befolgt habe.

Weiters erkläre ich, dass die elektronische und gedruckte Version der eingereichten wissenschaftlichen Abschlussarbeit formal und inhaltlich identisch sind.

Datum 20.11.2019

Marco Holzer

Unterschrift Verfasser/in
Marco Sebastian, Holzer

Abstract:

Gas sensing devices are widely used in various applications such as environmental monitoring, safety devices, smart applications, among others. Today's widespread chemiresistive gas sensors are based on semiconductive metal oxides that change their electrical resistance due to adsorption reactions of gas molecules on its surface. Despite some commercial success and the recent scientific interest, there is still a lack of methods to characterize the microstructure of the gas sensing materials during operation.

Within this thesis, a new approach to characterize gas sensing thin films by the means of Raman spectroscopy is conceived and applied. The designed Raman set-up enables the characterization of the microstructure and the electric properties of the gas sensing materials (CuO and ZnO) for different gas atmospheres. First, the author describes in detail the thin-film processing done by spray pyrolysis technique and photolithography for CuO and ZnO. Then, a detailed description of all included parts of the Raman setup and a manual for its assembly, including a proof of functionality, is provided. Finally, the set-up is used to investigate the interaction between target gases and metal oxide surfaces were in-situ by Raman spectroscopy. The obtained spectra of the metal oxide thin-films CuO and ZnO were studied and related to surface-gas interactions found in literature. The results demonstrate that Raman spectroscopy is a highly useful tool also for the in-situ measurement of very thin films used specifically for chemical sensors.

Acknowledgements:

This thesis was conducted at the Materials Center Leoben GmbH, Department Materials for Microelectronics, with the financial support provided by the project “FunkyNano – Optimierte Funktionalisierung von Nanosensoren zur Gasdetektion durch Screening von Hybrid-Nanopartikeln” (Österreichische Forschungsförderungsgesellschaft FFG, Grant No. 858637).

Greatest thanks go to my two supervisors, Priv.-Doz. Dr. Anton Köck and Priv.-Doz. Dr. Marco Deluca, who gave me the opportunity to write this thesis and whom I deeply admire for their knowledge and wisdom. Without their competent guidance, constant encouragement and valuable inputs, this work would have not been possible in this form. Moreover, they introduced me into scientific working several years ago. As I still utilise most of what I have learned from them in everyday life, for which I will be grateful my whole life.

I also want to thank Dr. Robert Wimmer-Teubenbacher for all the scientific discussions, helpful advices and for his relentless efforts to help me out. My sincere gratitude also goes to Vignaswaran Veerapandiyar as he not only gave constructive feedback on my ideas and measurement results, but also was there for me as a very good friend when needed. Thank both of you for making this thesis much more presentable!

In addition, I am very thankful for the continuous help and support of my colleagues Lisa Radl, Florentyna Sosada-Ludwikowska and Julien Magnien from MCL. They have always been ready to answer my questions and I greatly appreciate that.

I also want to mention Prof. Ronald J. Bakker at this point, whose Raman Lab is always open for young researchers and guests. Moreover, I am grateful for the financial support of the Montanuniversity Leoben, from which I kindly received the “Förderungsstipendium” – scholarship for this thesis.

Last but not least, I would like to thank my family members and numerous friends, who supported me throughout my work and studies. Without their love and appreciation, my accomplishments would have been impossible and worthless.

Contents

Abstract:.....	1
Acknowledgements:	2
1. Motivation.....	5
2. Theoretical Background	7
2.1 Metal-oxide Gas Sensors.....	7
2.1.1 Working principle	7
2.1.2 Solid-gas interactions	9
2.1.3 The Ionosorption Model.....	11
2.1.4 Metal-oxide semiconductor materials	13
2.2 Raman Spectroscopy.....	15
2.2.1 Introduction into Raman Spectroscopy.....	15
2.2.2 Raman scattering and selection rules	16
2.2.3 The Raman Spectrum	18
3. Experimental Part	22
3.1 Sample processing.....	22
3.1.1 <i>FunkyNano platform chip</i>	22
3.1.2 <i>Spray Pyrolysis</i>	23
3.1.3 <i>Photolithography</i>	25
3.2 Optical Characterization of the thin film samples	27
3.2.1 <i>Characterization of the MOx thin films by light microscopy</i>	27
3.2.2 <i>Interferometric measurement of thin film thickness</i>	27
3.3 The Raman set-up	28
3.3.1 <i>Gas supply system</i>	30
3.3.2 <i>Measurement Chamber</i>	31
3.3.3 <i>Electrical characterization</i>	33
3.3.4 <i>Raman spectrometer</i>	33
3.3.4 <i>Measurement procedure</i>	34
4. Results and Discussion	36
4.1 Metal-oxide thin film characterization	36
4.1.1 <i>Light Microscopy</i>	36
4.1.2 <i>Interferometric thickness measurement</i>	40
4.1.3 <i>Chemical Characterization of the thin-films by Raman</i>	40

4.2 In-operando Raman measurements	41
4.2.1 Proof of functionality – Raman measurements.....	41
4.2.2 Correlation between Raman spectra and the gas – MOx interaction.....	43
5 Summary and Outlook	49
6. List of Figures	50
8. List of Tables	51
9. References	52

1. Motivation

With the arrival of global warming and an imminent climate change as biggest threat to our planet, the need for environment-observing devices is becoming increasingly important and indispensable. Additionally, the monitoring of gases has become a requirement for many modern industrial processes and for providing human safety. Chemiresistive gas-sensors are a promising candidate for fulfilling the variety of such tasks and are therefore increasingly growing in importance.

In this work, a new experimental approach to study chemiresistive gas-sensors, which working principle is based on a change of the electrical resistance in metal oxides, will be introduced. This type of gas sensing devices can track various gases in our environment, with vision on miniaturization and smart application. Nevertheless, not all the chemical interactions between materials in use and target gases have been clarified yet. Although literature provides methods for analysing those interactions by the mean of rather complex and expensive measurement methods, there is a lack of structural methods analysing gas sensing materials non-destructively during operation. This work describes the design of an in-operando characterization set-up using Raman spectroscopy. For that, the measurement concept, a detailed description of used equipment and a proof of functionality will be presented. Finally, the author demonstrates how the obtained data can be used to extract valuable information about the materials structure and ongoing chemical interactions on the materials surface.

This thesis will mainly focus on following topics:

- First, the focus will be on the **processing** and optical characterization of gas-sensing samples based on metal oxide materials. For that, metal-oxide thin films are deposited on a provided platform chip by spray pyrolysis technique. Then, those films are structured by photolithography to obtain small gas-sensing samples, simulating a gas sensing device. Afterwards, they are characterized by the means of optical material characterization.
- Then, the basic scientific principles of **Raman spectroscopy** with all its advantages for thin film characterization will be discussed. As Raman spectroscopy is based on the interaction of laser light with the optical phonons of a material, it is a fingerprint of the investigated material, with signal only coming from a small, finite volume, in the range of a few micrometres. Therefore, the interactions between the surface of chemiresistive materials and target gases, which results into a structural change of the chemiresistive materials induced by chemisorption, can be detected by this method. Thus, it is well-suited to characterize gas-sensing thin films non-destructively.

The thesis is organized as follows:

- Part 1: Motivation
- Part 2: Theoretical Background:
First, the general principles of gas sensors and the special features of chemiresistive gas sensors, based on metal oxides, are presented. Then, the interaction between the gas sensing surfaces and target gases are studied. Last, a detailed introduction into the theory of Raman spectroscopy will be given. Moreover, the chapter explains several features of obtained Raman spectra and how those features can be related to structure and surface related effects of the gas sensing materials.
- Part 3: Experimental Part:
In part 3, a closer look on instrumentation, characterization and processing methods will be given. At the beginning, the processing of the gas sensing thin films deposited by spray pyrolysis is discussed. Additionally, it is explained how we can structure those films to obtain gas-sensing samples by photo lithography. Finally, the design of the in-operando thin-film characterization Raman setup and all its features will be described in detail
- Part 4: Results and Discussion:
Chapter 4 starts with the results obtained by the optical characterization of the metal oxide thin-films, which were produced by spray pyrolysis, structured by photolithography and later used as samples for in-operando Raman measurements. Different Raman measurements on thin films, accompanied by an electrical characterization, will proof the functionality of the provided concept. Moreover, a correlation between the Raman spectra of the materials, the microstructure and the interactions between different target gases and the metal oxide surfaces will be made.
- Part 5: Summary and Outlook:
The most important scientific insights and the impact of the work will be summarized within this chapter. In addition, possible application, improvements, future work and topics that should be further investigated in the future are presented.

2. Theoretical Background

This chapter introduces the basic scientific principles of chemiresistive gas sensors and the theoretical concept behind the new experimental approach based on Raman spectroscopy. The given introduction, considering the scope of the work, is needed to understand the experimental (chapter 3) and results and discussion (chapter 4) part, provided in this thesis.

2.1 Metal-oxide Gas Sensors

2.1.1 Working principle

Gas sensor devices are transducers that transform information about a specific gas and its concentration into a measurable electrical signal¹. Figure 1 shows the working principle schematically. A change in the gas concentration induces a change in the sensor signal, related to a change in the properties of the sensor material. For example, the presence of the hazardous gas carbon monoxide (CO) induces a change in the electrical resistance of a chemiresistive gas sensor, that is in the ideal case proportional to the amount of CO concentration in the environment. Several kind of gas sensors for different target gases have been developed and proposed¹. Some of them have been recognized as key devices to monitor, handle or control gases for various purposes². Therefore, gas sensors are used to guarantee personal safety, to monitor the environment and industrial processes.

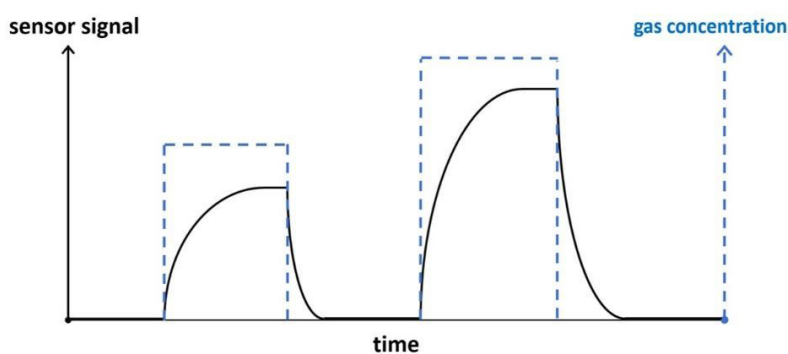


Figure 1: Working principle of a gas sensor device. A change in the gas concentration (dashed line) induces a proportional change in the sensor material (= sensor signal, full line)

For chemiresistive gas sensors, the electrical resistance changes drastically due to an interaction between the molecules of specific gases and the device. Whether the resistance increases or decreases, depends on the nature of the sensor material (n-type or p-type semiconductor) and the detected gas (reducing or oxidizing). A schematic of such a sensor is shown in Figure 2. Usually, a chemiresistive gas sensor device consists of a substrate as carrier for the gas-sensing layer. Every sensing unit consists of a micro-heater for operation at elevated temperatures and electrodes to apply voltage, enabling the measurement of the electrical resistance³. For the processing of such a structure, the use of thin film technology is needed.

This work will focus on the characterization of the gas-sensing materials cupric oxide (CuO) and zinc oxide (ZnO) used for this type of gas sensor devices and on their fabrication via spray pyrolysis technology, which is a simple thin film deposition method.

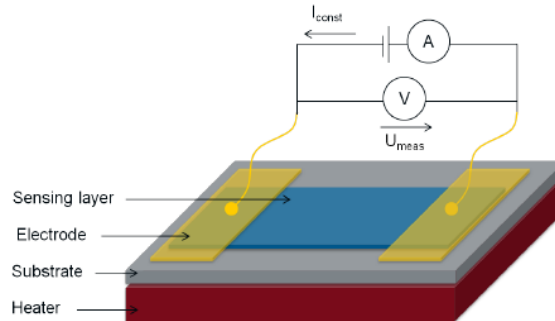


Figure 2: Schematic of a chemiresistive gas sensor based on metal oxide thin film by ⁴

Chemiresistive gas sensors are the most investigated devices among all types of gas sensors, with the majority based on metal oxide semiconductors (MOx), like CuO and ZnO. A possible explanation for this fact may arise looking at Table 1, that lists few of the advantages and disadvantages of MOx sensor materials¹. Commercial gas sensors require several 100 of Milliwatt for heating. However, the most important advantage is that metal oxides can be heterogeneously integrated into silicon microelectronics by post-processing technologies⁴. In other words, it is possible to have sensing layer, driving and read-out electronics on the same chip. Consequently, metal oxide materials are ideal for miniaturization and realization of smart sensor components¹.

Table 1: Advantages and Disadvantages of semiconductor MOx-based gas sensor devices employing micro hotplates

<ul style="list-style-type: none"> + High sensitivity to a broad range of gases + simplicity + operation speed and small size + heterogeneously integrable into CMOS technology + low cost fabrication 	<ul style="list-style-type: none"> - Sensitivity strongly depends on operation temperature (elevated temperatures, power consuming) - Drift in resistance and sensing properties over time - Lack of selectivity (suitable additives needed) - Long term stability
---	--

For the development, improvement and miniaturization of chemiresistive gas sensors and their materials, a sound understanding of the physics behind this technology is required. Thus, the next chapters will take a closer look on the interactions between gases and the surface of the gas-sensing materials.

2.1.2 Solid-gas interactions

Solid-gas interactions and other surface-related phenomena play a vital role for the function and understanding of gas sensing devices based on metal-oxide materials. As this work provides a new approach to characterize both material and its surface state simultaneously, it is essential to understand the different interaction mechanisms between a solid surface and gas molecules. In this chapter, the most important aspects of solid-gas interactions are introduced. Moreover, the charge transfer between adsorbates and metal oxide surfaces is described by presenting the ionosorption model in a later chapter.

According to Steinhauer, S.³, three different interaction mechanism between a solid surface (S) and gas molecules (G) are possible (see Figure 3), depending on the strength of the adsorption:

- Physical adsorption (physisorption):
The underlying forces of physisorption are electrostatic in nature, with nonreactive atoms and molecules. It relies on van-der-Waals dipole/dipole interactions and is therefore characterized by weak, long-range forces.
- Chemical adsorption (chemisorption):
This kind of adsorption involves the formation of chemical bonds between the gas molecules and the adsorbent. Additionally, and more importantly, it is accompanied by a charge transfer process. Since chemiresistive gas-sensors rely on a change in electric resistance for its sensing capability, which is coupled to the energy-band structure of a material⁵, chemisorption should be the predominant interaction mechanism.
- Non-reversible reactions:
Typically, a non-reversible reaction leads to the formation of a new compound. This kind of interaction is not desired during the gas sensor operation and should be avoided if possible.

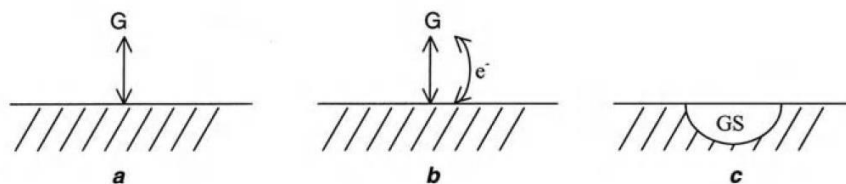


Figure 3: The different interaction mechanism between a gas and a solid, adopted by ⁶:
a) physisorption, b) chemisorption, c) non-reversible reaction

The interaction between gas molecules and solid surfaces can be described as the superposition of repulsive (interactions based on Coulombs law and the Pauli exclusion principle) and attractive (van der Waals interaction) forces and is dependent on the temperature⁷. Most commonly, the Lennard-Jones-Potential is used to approximate intermolecular interactions and is plotted in Figure 4 for adsorption. The potential can be written as⁸

$$V(r) = 4\epsilon \left\{ \left(\frac{r_0}{r} \right)^{12} - \left(\frac{r_0}{r} \right)^6 \right\}$$

Equation 1: Lennard-Jones Potential

with the intermolecular distance r and the parameter r_0 , which is the distance between the molecules at which the potential reaches its minimum. At r_0 , the function has the value $-\epsilon$, thus ϵ is equal to the minimum of potential energy $V(r)$. Due to the superscripts in the formula, it is often referred to as 12-6-potential.

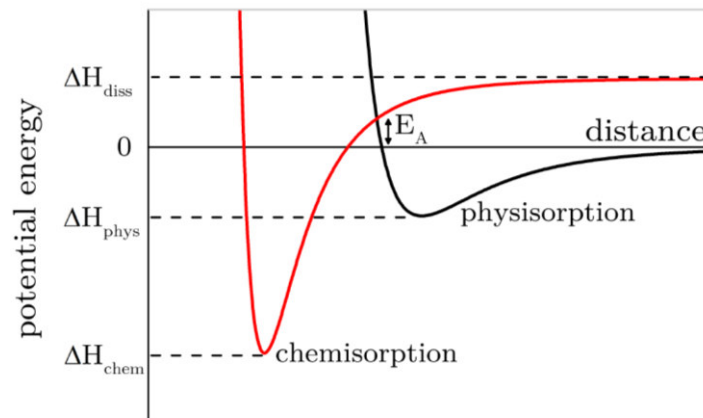


Figure 4: Lennard-Jones model for physisorption and chemisorption of a gas molecule adapted from the work of³

According to the work of Madou, M.J.⁹, the diagram in Figure 4 can be interpreted as follows:

- For physisorption, the energy of an approaching gas molecule is lowered due to dipole-dipole interactions and has its minimum at ΔH_{phys} . This process is exothermic with the heat of adsorption equal to the van der Waal binding energy. Therefore, physisorption will more likely occur for lower temperatures, which is characteristic for exothermic processes¹⁰
- For chemisorption, the impinging gas molecules dissociate. Thus, the potential energy approaches the value of ΔH_{diss} at large distances. Additionally, the minimum for chemisorption, ΔH_{chem} , is considerably lower and typically occurs at smaller distances. The surface coverage for chemisorption is therefore high at elevated temperatures and low at moderate temperatures, see also Figure 5.

As mentioned before, the Lennard-Jones potential (Figure 4) can explain and approximate the interaction between a pair of neutral atoms or molecules⁷. The case shown in Figure 4 is usually considered as activated chemisorption, since the lines for physisorption and chemisorption intersect at the positive energy value E_A , which is usually referred to as activation energy. This introduced concept is widely used to describe and approximate the nature of chemisorption of gas molecules on metal oxide semiconductors¹¹ because of its simplicity.

Because of the nature of solid-gas interactions, it is necessary to operate the gas sensing devices at elevated temperatures, for sensors to perform effectively. This is mainly because the density of molecules covering the surface via chemisorption is only high enough at elevated temperatures, as seen in Figure 5. Nevertheless, in case of using CMOS fabricated micro hotplates, there is a temperature limit of approximately of 400°C, as the thermal stability and degradation at high temperatures the temperature of use. This will be discussed in detail later.

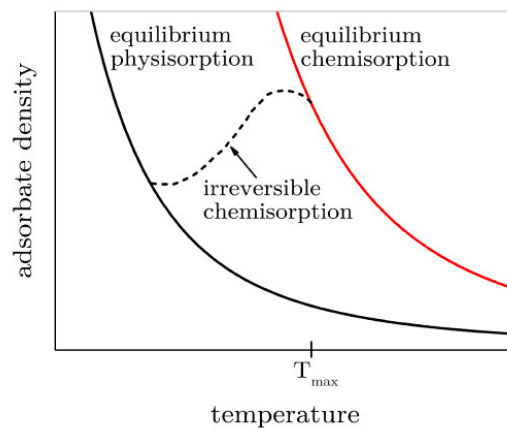


Figure 5: Density of adsorbed gas molecules as function of temperature, also provided by³

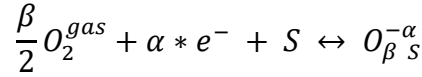
While the Lennard-Jones potential explains the adsorption of gas molecules on semiconductor surfaces well, it fails to describe the impact on the electrical properties of the material. Therefore, the Ionosorption model will be introduced.

2.1.3 The Ionosorption Model

As described in the previous chapter, a charge transfer process between adsorbate and adsorbent accompanies chemisorption. This charge transfer induces a significant change in the electrical properties of the gas-sensitive material, more precisely in the energy band structure⁵ of the material. For describing this effect, the Ionosorption model is commonly used in literature.

The work of Barsan, N. et al.¹² provides an in-depth explanation of the Ionosorption effect for metal oxides in different gas atmospheres. In this work, I will focus on the interaction of the metal-oxide semiconductors (CuO and ZnO) with oxygen as target gas:

1. The interaction with atmospheric oxygen results in ionosorption. The formed species of oxygen, molecular (O_2^-) or atomic (O^- , O^{--}), is dependent on temperature. The reaction can be written as



Equation 2: Ionosorption of a gas species

- (O_2^{gas} is an oxygen molecule in the ambient atmosphere, $O_{\beta}^{-\alpha} S$ is a chemisorbed oxygen species with $\alpha, \beta = 1, 2, \dots$, e^- is an electron and S an unoccupied chemisorption site)
2. The adsorbed oxygen is described as extrinsic surface acceptor state in the energy band representation. This state is negatively charged due to trapping of electrons.
 3. A space charge layer is formed, and the energy band bends upwards. This is shown in Figure 6 for both n- and p-type semiconductors.
 4. Depending on the type of semiconductor material, the electric resistance either increases or decreases:
 - a. For n-type metal-oxides, the conduction band will be depleted of majority carriers (electrons) and the electron transport from the bulk to surface is reduced due to the energy barrier eV_s , see Figure 6(a). Consequently, the electrical resistance increases
 - b. For p-type metal-oxides, the surface traps capture electrons from the valence band. This leads to an accumulation of majority carriers (holes) and therefore the electric resistance will decrease in the space charge layer
 5. The change in the electric resistance on the MOx sensor will then be measured by the sensor and related to the amount of oxygen in the atmosphere. This number will be calculated and displayed by the read-out electronics of the sensor in operation.

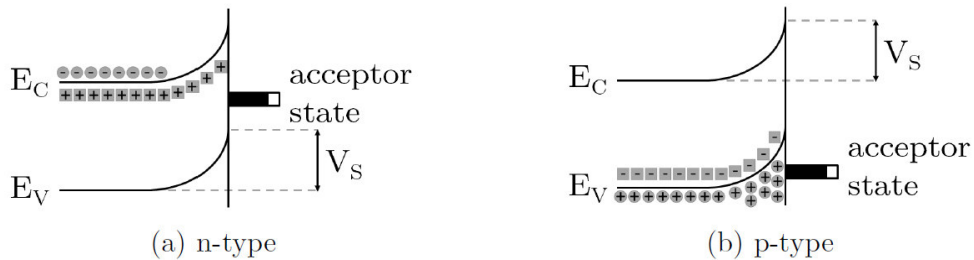


Figure 6: Bending of the energy band due to ionosorption of oxygen ³

The previous sections provide an overview of the concepts of ionosorption and energy band structures. Detailed reports can be found elsewhere in literature [^{13, 2, 5, 7, 14}]. These references and books are all worth a look for the interested reader.

Nevertheless, the given introduction, considering the scope of the work, will be enough to understand the experimental part (chapter 3) and the results and discussion part (chapter 4) of the thesis. Next, details about structure and properties of the thin film materials in study will be given.

2.1.4 Metal-oxide semiconductor materials

I) Zinc Oxide

Zinc Oxide, chemical formula ZnO, is a well-studied II^b-IV compound semiconductor that usually crystallises in the hexagonal wurtzite structure, shown in Figure 7. Due to its wide band gap, ZnO is transparent in the visible part of the electromagnetic spectrum. Therefore, it can be used as a transparent conducting oxide (TCO) or as contact for solar cells¹⁵. Moreover, it is reported to be a gas-sensing material, since the surface conductivity is strongly influenced by the presence of various gases¹⁶. Forthcoming applications and visions can be found in the book of Klingshirn, C., et al.¹⁷, that also provides a deep insight into the fundamental properties of ZnO and its technologies.

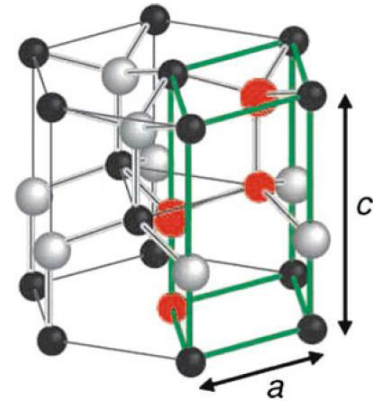


Figure 7: Hexagonal wurtzite-type lattice. The primitive unit cell is marked by green lines. The atoms of the molecular base unit ($2x$ ZnO) are marked by red full circles¹⁷.

Table 2, adopted from¹⁷, summarizes the most important material properties of ZnO, concerning this work:

Table 2: Properties of ZnO

Crystal structure	Lattice parameters [nm]	Space group	Point group	Density [g/cm ³]	Band gap [eV]	Conduction mechanism	Melting point [K]
Wurtzite	a = b = 0,3249 c = 0,52042	P6 ₃ mc	6mm	5,675	3.4 eV	n-type (electrons)	2242

II) Cupric Oxide

Cupric Oxide or Copper(II)-oxide, with the chemical formula CuO, has attracted much interest for its application as photothermal or photoconductive material. In addition, it is also the basis for several high T_C superconductors¹⁸. Latest reports show that CuO thin films can be used for gas sensing applications¹⁹. The knowledge of such gas-sensing studies is applied within this master thesis.

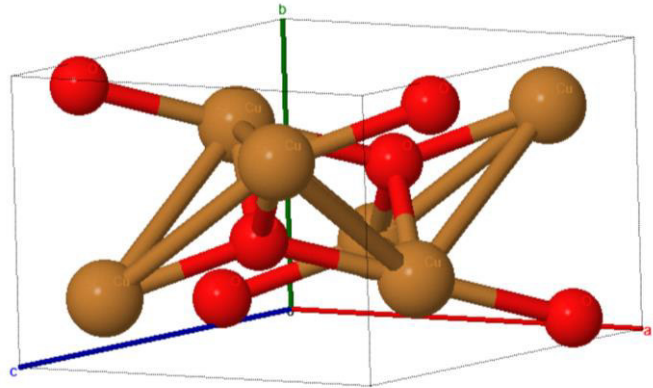


Figure 8: The unit cell of the complex monoclinic lattice. The figure was drawn with the web application by²⁰.

While Figure 8 shows the complex crystal structure of CuO, Table 3 lists data relevant for this thesis.

Table 3: Properties of CuO. Crystal structure, lattice parameter, space and point group were provided by²¹. The data for the density and the melting point were taken from²², while information about the electrical properties, conduction mechanism and band gap value, given by²³.

Crystal structure	Lattice parameters [nm]	Space group	Point group	Density [g/cm ³]	Band gap [eV]	Conduction mechanism	Melting point [K]
Monoclinic	a = 0,4684 b = 3,423 c = 0,513 $\alpha = \gamma = 90^\circ$ $\beta = 99,54^\circ$	C _{6h} ²	2/m	5,675	3.4	p-type (holes)	2242

2.2 Raman Spectroscopy

2.2.1 Introduction into Raman Spectroscopy

Raman Spectroscopy (RS) is an optical characterization technique based on Raman scattering, which describes the inelastic scattering of light by matter. Typically, the photons of the incident light are scattered with its photon energy reduced or increased by a vibrational quantum of the scattered atom/molecule²⁴. Consequently, the obtained spectrum is a fingerprint of the investigated material. Over the last decades, Raman scattering has proven to be a powerful non-destructive material characterization technique in the field of materials science. It can be used to study defect inhomogeneities, dopant profiles, local strains, crystallinity, the electronic structure of the material and many more²⁵.

In contrast to other light scattering methods, like x-ray scattering for instance, where an average of sample properties is obtained, Raman scattering is a local probe with signal coming from a small, finite volume of the material²⁵. The reason for that is the use of a laser source for light radiation, resulting in a small interaction volume. As the Raman effect is inherently weak, typically 10^{-8} of the intensity of the incident exciting radiation, a monochromatic light source with high intensity, must be used²⁶. Figure 10 illustrates the exceptionally high axial and lateral resolution, obtained by using a Laser light source for RS. For a green laser ($\lambda = 532\text{nm}$) and an objective with $NA = 0.9$, for example, the spot size is approximately $0.7 \mu\text{m}$ and the penetration depth $2.2 \mu\text{m}$. Consequently, the Raman spectroscopy is well suited to analyse thin films, small devices and surface related phenomena.

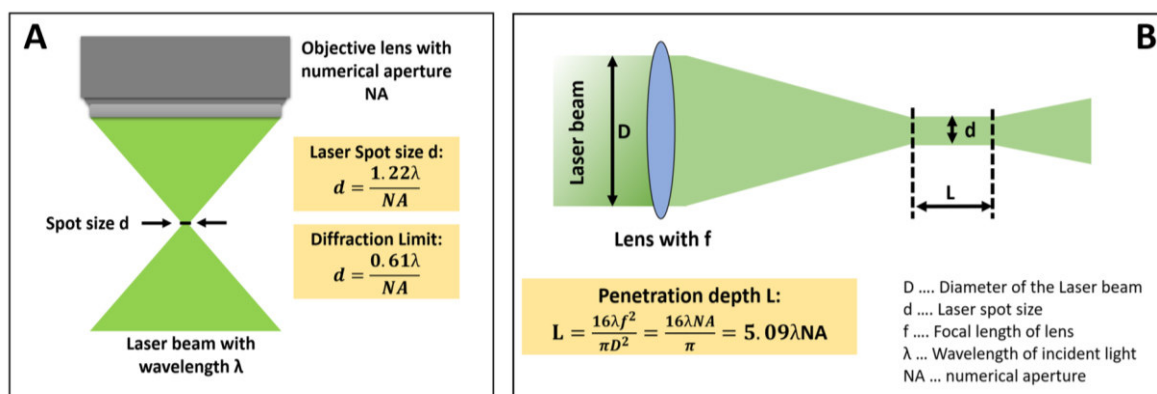


Figure 9: Schematics and formula for the lateral (A) and axial (B) resolution of the incident laser beam adopted by^{26,27}. Given formulas are just for approximation, as they do not include material constants and light-matter interaction as absorption.

The aim of this work is to design a measurement setup that allows to characterize the interactions between various gases and the surface of semiconductor materials at different temperatures and atmospheres. Additionally, the inclusion of an in-operando resistance measurement for electrical characterization of the sensor-device would be beneficial. The authors of^{28, 29, 30} proofed that such a set-up is feasible and that similar concepts are working well. But before heading to the experimental part, a closer look on the Raman effect is required.

2.2.2 Raman scattering and selection rules

The Raman effect or Raman scattering is a complex physical effect that can be explained by studying light-matter interactions, condensed matter physics, quantum mechanics and crystal symmetry. The detailed laws of this phenomenon and the corresponding formulas can be found in further literature and references (e.g., Refs.^{7,31-35}). However, the following paragraph revises the most important points, obtained by referred literature.

When monochromatic light impinges on matter, light/atom-vibration interaction leads to elastic scattering (called Rayleigh scattering) + (acoustic/optic) inelastic scattering (called Brillouin/Raman scattering) + upper terms (e.g. Hyper Raman effect). The acoustic Brillouin scattering is observed at very low energy ranges for crystalline material and its observation requires sophisticated measurement set-up and equipment. The optic Raman scattering on the contrary, contains two groups of transition symmetric versus the exciting phonon energies that can be seen in RS:

- so-called Stokes transition with the incident laser losing energy to matter, resulting from the fundamental vibrational level
- Anti-Stokes transition with light receiving energy from matter, resulting from the upper vibrational levels

Figure 10 (a) shows the different scattering processes from energetical point of view. It also shows a typical Intensity vs. Raman shift plot, used for RS, in Figure 10 (b). The Raman shift is defined as:

$$raman\ shift = \Delta\tilde{\nu} = -\left(\frac{1}{\lambda_0} - \frac{1}{\lambda_i}\right)$$

Equation 3: Raman Shift

with the incident laser wavelength λ_0 and the Raman spectrum wavelength λ_i . At room temperature, the Stokes process is more probable due to the larger population of ground vibrational states with respect to higher vibrational states.

For a three-dimensional solid containing N unit cells with p atoms inside, $N(3p-6)$ different phonons can propagate and their wavevector (\vec{k}) all point in a volume of the reciprocal space called Brillouin zone (BZ). There are two types of phonons/branches, depending on frequency and direction of vibration. The acoustic branch has $3N$ modes, while the remaining $3(p-1)N$ degrees of freedom belong to the optical branch. Depending on whether the optical phonons move parallel or perpendicular to the direction of wave propagation given by \vec{k} , the optical phonons are referred to as being longitudinal (LO) or transversal (TO). The BZ describes the geometrical distribution of the wavevectors in the reciprocal space similarly to a unit cell describing geometry and periodicity of a crystal in the direct space. Thus, group theory and symmetry considerations give information on the number of Raman-active phonons³⁵. The calculation of the Raman-active modes is generally done in crystallographic works, referred to as selection rules. A simple way to calculate the phonon modes for a given point group is offered by the Bilbao Crystallographic Server³⁶. The developed model, however, is only valid for a perfect crystal and real spectra, obtained by experiments and may differ from the

predicted ones. First, interactions between different phonon branches result in the appearance of additional second order peaks. Second, in presence of disorder, phase mixture or defects, the considerations are also not valid anymore and can lead to a change in spectra. This is referred to as selection rule breaking and results in a higher number of Raman peaks as predicted.

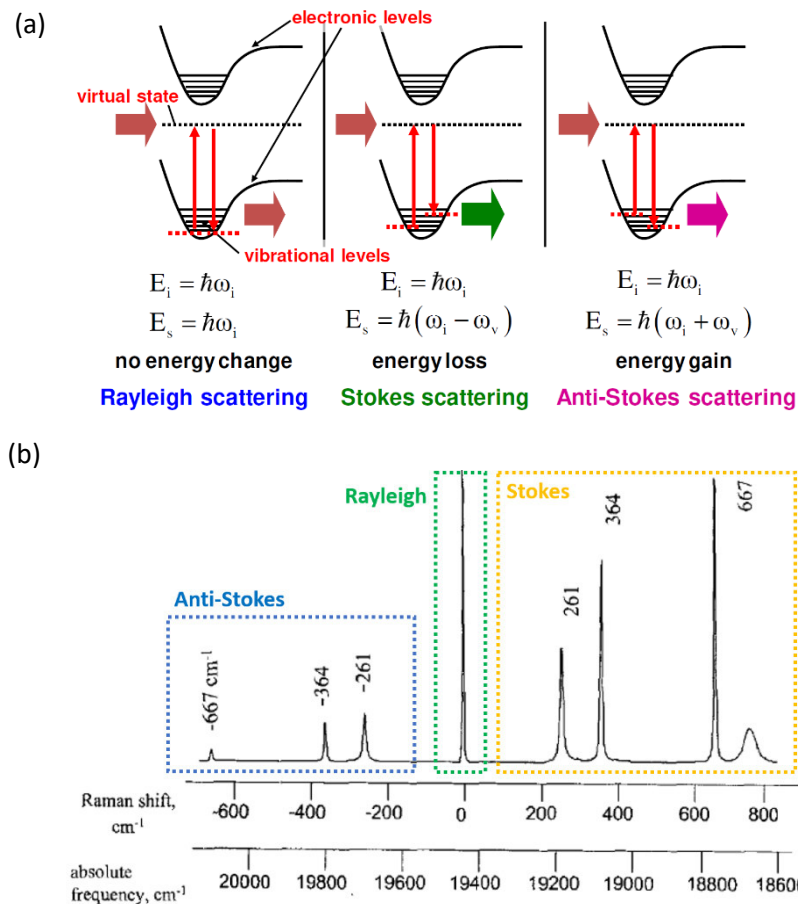


Figure 10: (a) Schematic showing the Raman effect from a quantum mechanical point of view⁵⁶. (b) The room-temperature Raman spectrum of CCl_4 with plotted spectral lines belonging to different scattering processes. Figure adopted by²⁷.

To conclude, it was shown that the Raman effect is strongly bound to a materials crystal- and microstructure. By applying the Raman selection rules for a certain point group and studying the related phonon modes with all its atoms/molecules/characteristics included, valuable information about the microstructure of the material in study can be extracted.

2.2.3 The Raman Spectrum

The previous chapter explained the Raman effect and how the Raman-active modes for different materials are determined. In addition, it was explained how a Raman spectrum of a material can inform both on the chemistry (chemical bonding, composition, second phases), the structure (symmetry, space group, disorder/coherence length) and the physics (charge transfer, stress, phase transitions) of a solid³⁴. For this procedure, however, the different features of a Raman spectrum must be analysed.

Usually, the Raman spectrum is represented as frequency shift from the incident light (= Raman shift) vs. gathered intensity. The Stokes shift (lower-energy) is measured and displayed as positive shift by convention, see equation 3. The most important parameters in a Raman spectrum, see Figure 11, and which information they bear, is summarized as follows²⁷:

- **Peak position:**
Depends on the strength of the atomic bond and is influenced by any changes in the bond distance or strength. It is related to atomic mass, electrostatic forces, strain, hybridization, etc.
- **Peak Intensity:**
Depends on the polarizability of the bond and is influenced by any changes in phase amount, crystal orientation and by charge transfers.
- **Peak width:**
The peak width, defined as full width at half maximum (FWHM), depends on the coherency of the vibration. It is influenced by temperature and disorder effects. A single crystal will give sharp peaks, while an amorphous material results in broad peaks.

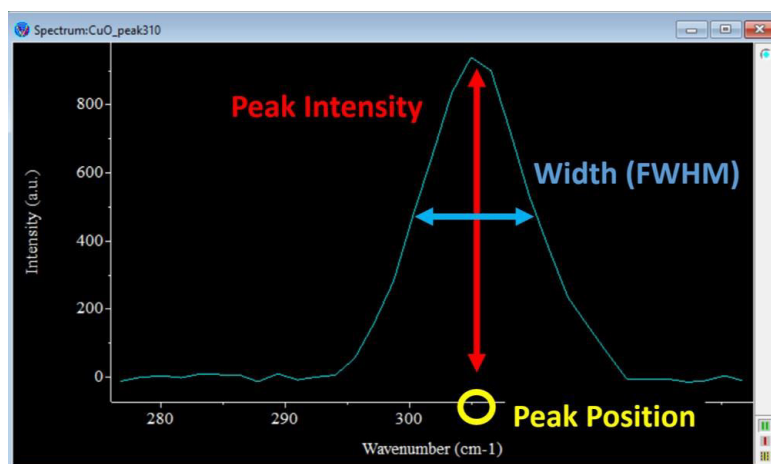


Figure 11: Measured Raman peak of CuO with important parameters schematically shown. The fitting of the curve and determination of the parameters is carried out with the help of suitable programs.

To predict the Raman spectra of a material and its features, the user must apply the selection rules for the semiconductor materials in study and their related crystal symmetry. This is done by using the Bilbao Crystallographic Server³⁶. Later the results are compared with spectra given by literature^{37,38}. In the next step, these are compared to the actual measurement data to extract information. This process is discussed in the results section of this thesis.

Nevertheless, as the gas-sensing layers of CuO and ZnO are only few hundred nanometres thick, it is expected that the obtained spectra differ from the predicted spectra. Moreover, the measured intensities will be lower and therefore the measurement times higher. Possible changes and their origin will be discussed after providing the spectra of the gas-sensing semiconductor materials in short. For both CuO and ZnO, the Raman spectrum with all its peaks and features is given. Additionally, the origin of peaks is given by the Raman selection rules.

Raman spectra of materials in study + applied selection Rules:

I) Raman spectrum of CuO:

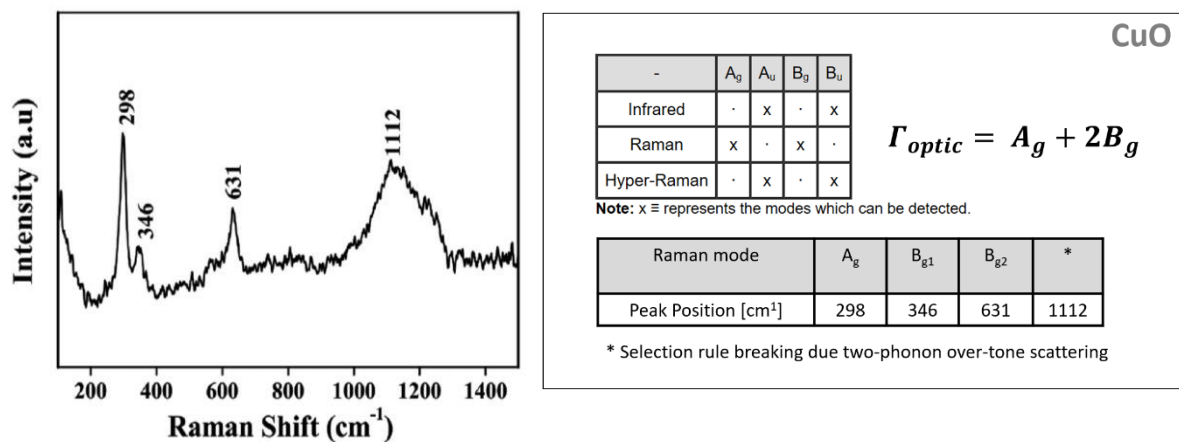


Figure 12: Raman spectrum of CuO measured Dolai, S., et. al⁵⁷ at room temperature. On the left, the Raman spectrum with the 4 characteristic peaks is given, while on the right, the application of the Raman selection rules is shown.

II) Raman Spectrum of ZnO:

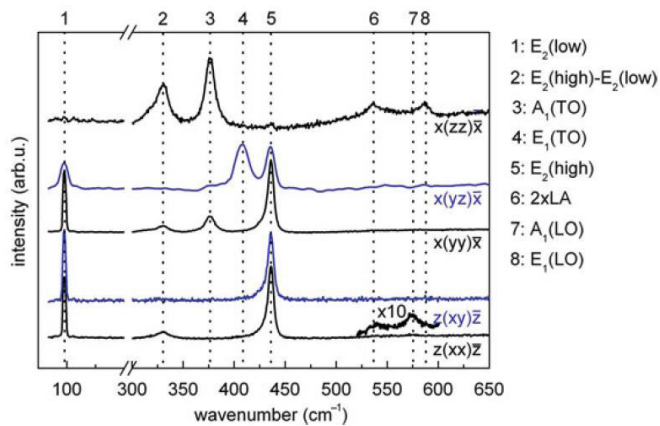


Figure 13: Raman spectrum of ZnO at room temperature for various scattering configurations done on a single crystal¹⁵, shown on the left. The spectrum for a polycrystalline ZnO is the sum of the spectra. Peaks 2 and 6 cannot be predicted by selection rules (second order effects and rule breaking). Calculation of the Raman active peaks is shown below.

ZnO						
-	A ₁	A ₂	B ₁	B ₂	E ₂	E ₁
Infrared	x	·	·	·	·	x
Raman	x	·	·	·	x	x
Hyper-Raman	x	x	x	x	x	x

Note: x ≡ represents the modes which can be detected.

$$\Gamma_{\text{optic}} = 2A_1 + 2E_1 + 2E_2$$

Raman mode	A ₁ (TO)	A ₁ (LO)	E ₁ (TO)	E ₁ (LO)	E _{2,low}	E _{2,high}
Peak Position [cm ⁻¹]	378	574	410	590	99	438

III) Spectra of the materials deposited on the substrate/chip:

The spectra of CuO (Figure 12) and ZnO (Figure 13) are obtained by measuring bulk material samples. Due to the design of the device and the presence of other materials lying underneath the deposited metal-oxide thin films, the Raman spectra will change as follows:

- There will be an overlap between the signal of the metal-oxide thin films and the materials of the device³⁹, as the penetration depth is bigger than the layer thickness. A similar situation is shown in Figure 14. Moreover, the spectra of the most used CMOS materials (Si and SiO₂) are shown in Figure 15.
- Intensities of some Raman peaks may be lowered or even completely suppressed by the signal of the substrate material (Si, SiO₂ for this work). On the other hand, there can be new peaks appearing due to a symmetry change of the material or selection rule breaking.
- Peak positions can shift due to presence of residual stresses in the different layers, new phases or other changes related to the strength of the atomic bond.

- The possible presence of vacancies or other defects will influence and change the Raman spectra. For example, the ZnO broad peak between 180cm^{-1} and 250cm^{-1} , that is not present in Figure 14, but in Figure 15, is associated with oxygen vacancies³⁹.

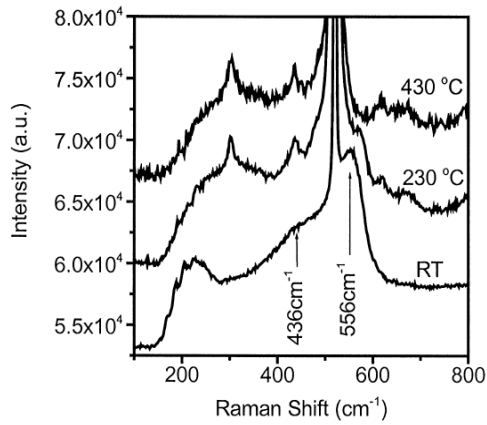


Figure 14: Raman spectra of ZnO thin films on a (0 0 1)-Si substrate³⁹ for different temperatures. The temperature dependence of the RS can be clearly seen.

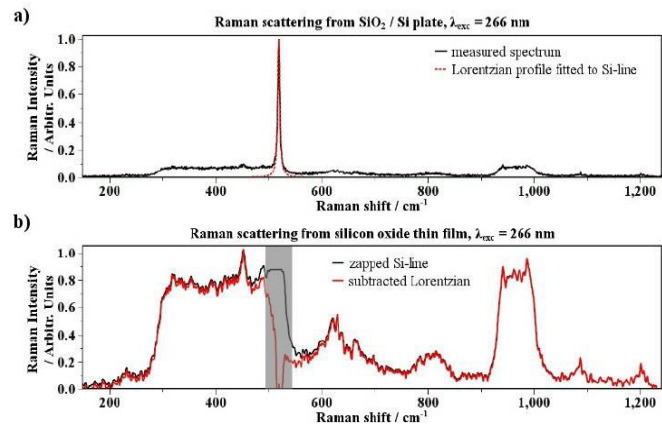


Figure 15: Raman spectra of silicon (a) with its characteristic sharp peak near 520cm^{-1} and second order broad peaks. In (b), the broad spectrum of SiO_2 can be seen⁴⁰. The red line represents the fitting curve of the measured spectra, represented by the black line.

3. Experimental Part

Finally, this chapter will present the design and measurement set-up of the in-operando gas-sensor characterization by Raman spectroscopy. However, to proof the functionality of the construction, clean, high-quality samples must be produced first to exclude measurement uncertainties or artefacts. Thus, a reliable processing technique with optimal set-up parameters is needed and will be provided within this chapter. As seen in the schematic workflow of Figure X.16, the author will also discuss used instrumentation and its purpose in detail.

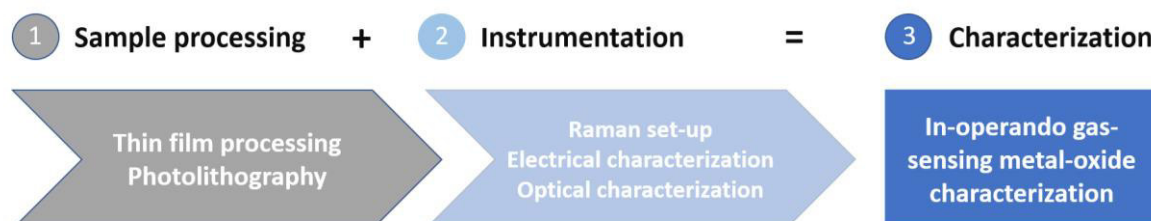


Figure 16: Workflow towards the in-operando characterization of the gas-sensing metal-oxide thin films within this thesis.

3.1 Sample processing

To proof the functionality of the in-operando gas-sensor characterization system, gas-sensor-imitating samples are needed. The deposition was done by spray pyrolysis technique because of its simplicity and low cost. In general, electric resistance measurements require a certain platform chip system underneath the gas-sensing metal-oxide layer, with an implemented electrode system, to apply voltage and measure the resistance via a 2- or 4-point resistance measurement. For that, metal-oxide thin films were deposited on a platform chip, which was provided by the ams AG within this funded project, see Figure 17 and 3.1.1.

3.1.1 FunkyNano platform chip

The provided so called FunkyNano chip with an incorporated electrode system for the realization of gas sensor structures is shown in Figure 17. A FunkyNano chip contains 16 separate gas-sensing structures, each consisting of 4 platinum electrodes, which will be later connected by the conductive metal-oxide thin-films. Both ZnO and CuO thin films were deposited on these chips, built up from several layers. The top layer is a 1000 nm SiO₂ insulation layer including 200 nm thick platinum electrodes, added on a 5 nm titanium adhesion layer, supported by silicon as base material on the bottom of the chip.

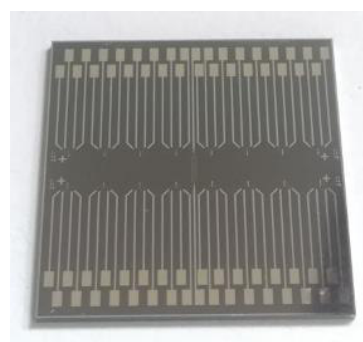


Figure 17: 2x2 cm FunkyNano platform chip provided by ams AG. The platform chip has a thickness of 0,74 mm

3.1.2 Spray Pyrolysis

Spray pyrolysis is a thin film deposition technique, suitable for the deposition of metal oxides. It is based on very simple equipment, does not require vacuum conditions and has low operational costs. Therefore, spray pyrolysis is considered as an attractive alternative to physical vapor depositions (PVD) techniques, that are usually used for thin-film deposition^{41,42}.

In the excellent work of Mutinati, G.¹, the spray pyrolysis technique is described as follows: A typical spray pyrolysis set-up consists of an atomizer, precursor solution, carrier gas, substrate heater and a temperature controller. For a better visualization, the set-up in use is shown in Figure 18. In the process, a precursor solution, that contains all the necessary elements to determine the chemical composition, is atomized and sprayed on a heated substrate. In order to atomize the liquid solution into a fine mist, a certain pressure ($p_{N_2, \text{atom}}$) must be applied. To guarantee a constant supply of substrate in the nozzle, additional gas pressure ($p_{N_2, \text{flask}}$) is applied to the solution in the flask. After atomization, the mist is transported towards the heated substrate by a carrier gas ($p_{N_2, \text{carrier}}$). The desired solid material forms on the substrate as the components of the solution react at or close to the surface. While Table 4 itemizes the used equipment, Table 5 overviews several parameters used for spraying.

At this point, the author would like to point out that all the experiments were carried out in a chemical lab fulfilling necessary safety requirements and under the presence of a fume hood. Especially the precursor substances can be hazardous and must be handled carefully.

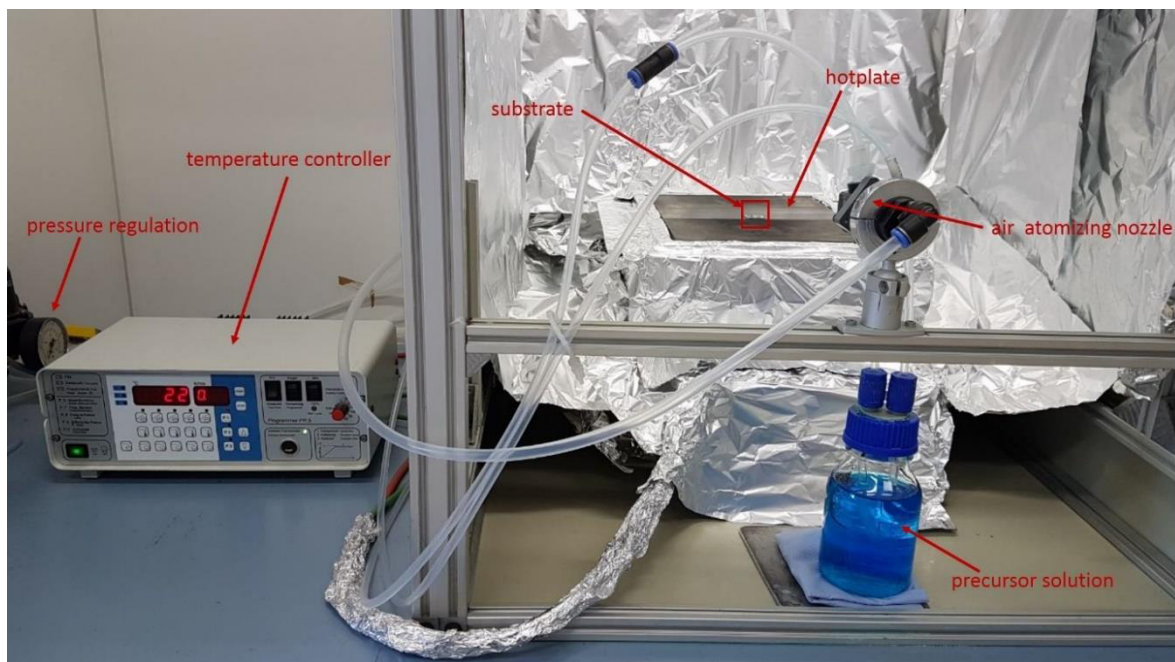


Figure 18: Spray pyrolysis set-up at MCL Forschungs GmbH with courtesy to⁴³

Table 4: Different equipment parts for spray pyrolysis set-up listed

Equipment	Manufacturer	Description
Hotplate	PZ28-ET, Harry Gestigkeit GmbH	A high-temperature titanium hotplate for heating of the substrate
Temperature Controller	PR5 3T, Harry Gestigkeit GmbH	To control the the temperature of the hotplate accurately
Precursor solution reservoir	Lactan (Erlenmayer flask)	For storing the solution. The glass reservoir should withstand applied pressures
Air atomizing nozzle	Quickmist 1/4 QMJ with flat air cap SUQR220B	Atomizes the precursor solution into fine droplets
Gas supply with pressure regulation	2x pressure reducer valve and regulator by Linde GmbH, N ₂ gas from Linde GmbH	Supplies spray pyrolysis set-up with carrier gas, flask pressure and pressure for atomization
Miscellaneous	PFA flexible tubing and connectors by Swagelok Company, aluminium foil	Tubes to connect and supply different parts. Aluminium foil to protect equipment

Table 5: Spray Pyrolysis process parameters for the different materials (ZnO, CuO)

Process parameter	ZnO	CuO
Precursor solution	0.1M Zn(CH ₃ COO) ₂	0.3M Cu(NO ₃) ₂
Solvent	Ethanol	Distilled water
Chemical reaction	Zn(CH ₃ COO) ₂ (l) $\xrightarrow{\text{heat}}$ 4ZnO (s) + 6CH ₃ COOH (g)	Cu(NO ₃) ₂ ·3H ₂ O (l) $\xrightarrow{\text{heat}}$ CuO (s) + 2CH ₃ COOH (g)
Temperature [°C]	400	
Substrate	FunkyNano Chip and SiO ₂ reference platelets(*)	
Pressure carrier gas [bar]	p _{N₂,carrier} ≈ 1.1	
Pressure in flask (p _{N₂,flask}) [bar]	0.15	1
Atomization pressure (p _{N₂,atom}) [bar]	1.5	0.3
Spray time	16 x 30 s	4 x 10 min

(*) for film thickness measurements

After the spraying process, all samples were annealed for 30 min at 400°C to obtain crystalline samples. This was done on the hotplate of the spray pyrolysis set-up in ambient air.

3.1.3 Photolithography

The next step in the sample processing is to pattern the deposited metal-oxide layers by photolithography. Photolithography is a process used in microfabrication to transfer specific pattern and designs into a functional layer (MOx) or layer⁴⁴. This process is schematically shown in Figure 19.

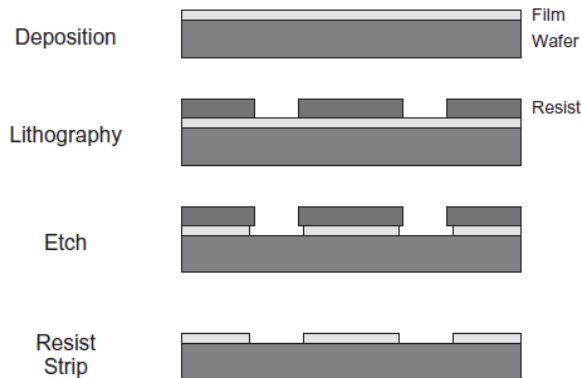


Figure 19: Photolithography as a simple subtractive patterning process⁴⁴

For this thesis, Photolithography is used to pattern parts of the deposited gas-sensing thin films between the platinum electrodes of the FunkyNano chip. This process consists of several steps, as seen in the process scheme in Figure 20. Detailed description of the equipment and chosen set-up can be found in Table 6.

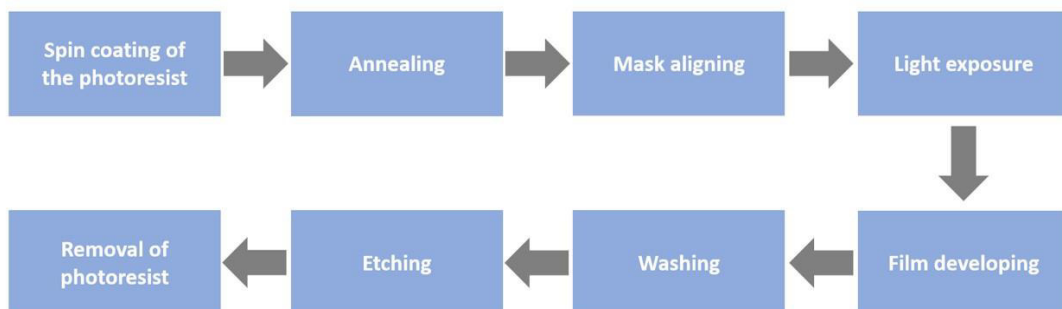


Figure 20: Process scheme of the photolithography process

Table 6: Photolithography set-up with short explanation of the individual steps. For a detailed description of the whole process, the literature reference of⁴⁴ is highly recommended.

Process step	Equipment and set-up	Description
Spin coating of the photoresist	Spin Coater Model 4000, Electronic Micro Systems LTD set-up: 30 s at 4000 rpm with acceleration rate of 5000 rpm/s	Deposition of the positive photoresist (AZ Mir 701, MicroChemicals GmbH)
Annealing	100°C for 60s	Removes the solvent from the spun-on resist and improves the adhesion + reduction of residual stress
Mask-aligning	Manual mask aligner MJB4 (Suss Microtec) + FunkyNano photomask (MCL Forschung GmbH, ams AG)	Applies photomask on the substrate and defines which areas of the resist surface will be exposed and which will be covered from light radiation
Light exposure	UV irradiation for 13.1s Light intensity = 13.6 W/m ²	Irradiated regions of the photoresist will become soluble in the developer
Development	AZ 726 MIF Developer (Merck) 60s	The development process involves chemical reactions wherein unprotected parts of the resist get dissolved in the developer
Washing	With distilled water	Stops development process
Etching	CuO: 6M HCl for 2.5min ZnO: dry physical etching with Ar ions (IonSys 500, Roth und Rau AG, AIT Vienna)	Removal of the undesired metal oxide material
Removal of photoresist	CuO: acetone for 20min	Removal of the photoresist and exposure of the remaining pattern

3.2 Optical Characterization of the thin film samples

After processing, the deposited metal-oxide thin films were characterized. For this purpose, the samples were examined by the means of light microscopy, followed by an interferometric thickness measurement. In addition to that, the chemical composition of the sprayed material was studied by Raman spectroscopy. The instrumentation for Raman spectroscopy is described in full detail later.

3.2.1 Characterization of the MOx thin films by light microscopy

The deposited metal-oxide thin-films were characterized by using a Zeiss AX10 Imager light microscopy in brightfield mode. Objectives with different magnification (10x, 20x and 50x, respectively) were used. In addition, a Nikon ShuttlePix P-400R digital microscope produced images with even lower magnification.

The technique of light microscopy is essential to take a closer look on the structure of the samples, as well for processing control. Only homogeneously deposited and well-structured films will produce sound results for Raman spectroscopy and the 4-point resistance measurement. Moreover, it is necessary to look at the samples in between the different processing steps to evaluate important process parameters (e.g.: etching time of the structured samples). For this reason, the use of such instruments is mandatory.

3.2.2 Interferometric measurement of thin film thickness

A Filmetrics F40 thin film analyser was attached to the Zeiss AX10 microscope to measure the film thickness. For Raman measurements, only films with the thickness of a few tenths of a micron will give enough rise to Raman spectrum, producing a satisfying signal-to-noise-ratio. For conductometric sensor devices, the sample thickness should be rather small (e.g. 50-150 nm), in order to optimize the surface-to-volume ratio of the gas sensor. However, for the measurement concept of this thesis, it is better to use slightly thicker samples to gather higher MOx intensities. This leading to a better signal-noise ratio and prevents too much influence of the silicon substrate on the spectra.

To indicate the thickness of the sprayed layer, a SiO₂-platelet with known thickness is used as substrate and reference sample. Figure 21 shows such a SiO₂ sample beside the FunkyNano platform chips, right after spraying process. The SiO₂ layer of the platelet is 480nm thick. After depositing the metal oxide thin film on the substrate, the sample is measured again. The thickness at several positions was measured, using the provided software (FILMeasure 6) and averaged for statistical reasons.

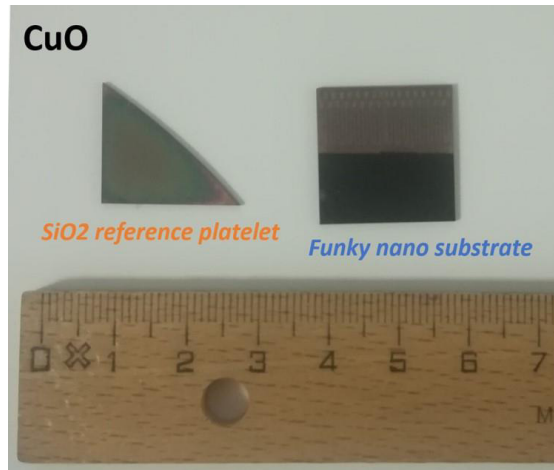


Figure 21: CuO thin film on SiO₂ reference platelet (left) with FunkyNano samples (right) beside. The photo was taken right after the spray pyrolysis process.

3.3 The Raman set-up

To characterize the metal-oxide thin films samples by Raman Spectroscopy in operation, a functional design must include following features:

1. Gas supply system:

To study the interactions between the sensor materials surface and the target gases, a constant gas supply and atmosphere must be guaranteed. Additionally, safety requirements must be fulfilled and the possibility to change or mix target gases manually is desired.

2. Measurement Chamber:

The measurement chamber must include a sample holder, a connection to the gas supply, ports for electronic cables, a glass window for the laser and a temperature control unit. Moreover, the design should allow the operation at elevated temperatures up to 350°C.

3. Electrical characterization:

Usually, an electric resistance measurement (2- or 4-point, depending on the influence of contact resistance) is used for the electrical characterization of chemiresistive gas sensors and their materials⁴. To combine the electrical setup with the Raman spectrometer, contact test leads and BNC connectors are used. They connect the sensing sample inside the Raman chamber with a source meter unit (SMU), a powerful instrument suited for several kinds of electrical measurements, and a computer with special software.

4. Raman spectrometer:

It is the most important instrument of the overall setup. The instrument measures the frequency shift in the laser light induced by the material. The large and heavy spectrometer is the only locally fixed instrument in this assembly. Therefore, all other parts of the setup should be moveable and attachable to different instruments and spectrometers.

A sketch of the designed setup is presented in Figure 22. One of the main advantages of the setup is its movability. Except the Raman spectrometer, all the parts can be stored and transported with little effort. If necessary, special gas bottles with little volume and weight (e.g. 10 litres) can be ordered and connected to the transportable setup.

Moreover, the set-up can be attached and applied to other types of optical characterization methods, like photoluminescence spectroscopy, for instance. Normally, Raman spectrometer can perform photoluminescence measurements⁴⁵ as well. However, for the materials in study, either the energy of the available light source was not high enough to stimulate electrons (for ZnO bandgap higher than Laser energy, need of UV laser) or the spectral lines were out of the spectrometer range (for CuO, spectrometer with different grating is needed).

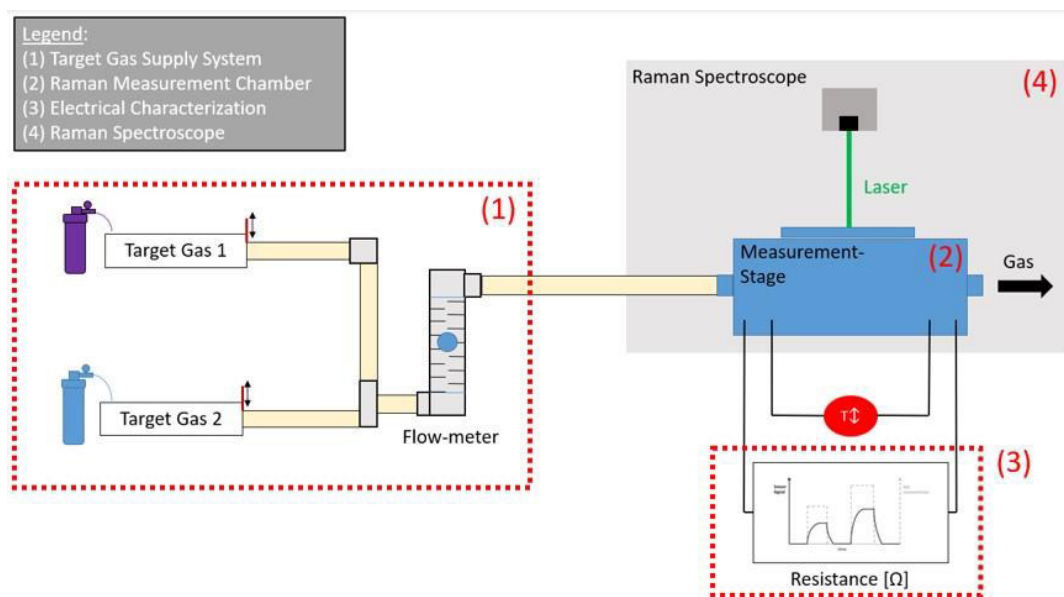


Figure 22: A schematic sketch of the overall measurement setup, consisting of different parts

Compared to the schematic sketch of Figure 22, the Figure 23 shows the real Raman set-up in the lab. On the left, the different target gas bottles can be seen. Tubes connect the gas supply to the measurement stage, which can be temperature controlled and attached to the Raman spectrometer. On the right, a source meter unit (SMU) with suitable software is located. It is connected to the measurement chamber and sample via cables. On the desk, the heart of the setup, a Horiba Jobin Yvon Labram300 Raman spectrometer, can be seen. Additionally, flow meter units could be used to create specific gas atmospheres with certain concentrations.



Figure 23: The in-operando gas sensing metal-oxide characterization setup with a special measurement chamber including a Raman spectrometer, gas supply, measurement chamber and electric resistance measurement

The next paragraphs will list all the different parts and functions of the equipment. Furthermore, the sample mounting and connecting to the electrical measurement will be explained in detail. Finally, the author describes the features of the Horiba Jobin Yvon Labram300 Raman spectrometer.

3.3.1 Gas supply system

The list of equipment for providing a certain target gas to the measurement chamber, adjusting its pressure and flow rate is given in Table 7. Both Figure 24 and 25 show the different parts of the instrumentation for better visualization.

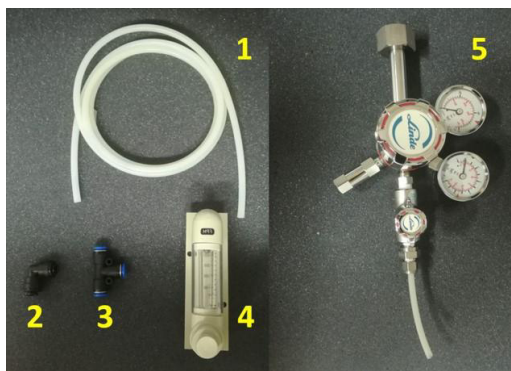


Figure 24: Different parts of the gas supply system according to numbering according to Table 7



Figure 25: Nitrogen and synthetic air gas bottles provided by Linde GmbH

Table 7: Equipment listed for the gas supply system

Number	Name/Equipment	Description
1	Flexible polymer tubes (Swagelok Company PFA_T6M_1M) 3 metre cut into 6 pieces	Transports target gas towards measurement chamber
2	2x Connectors (Swagelok Connectors suited for 6mm)	Links flexible polymer tubes
3	1x T-Connector (Swagelok Company suited for 6mm)	Connects the two attached target gas paths, if mixing of gases is needed
3*	Optional: 2x mass-flow controller (for example Bürkert 8715)	Mass-flow controllers can be used to provide a specific gas concentration by mixing
4	1x flow-meter (producer unknown)	Regulates flow rate
5	2x Pressure reducer + Closing Cap 1 for each gas (N ₂ , synthetic air) (Linde GmbH)	Reduces the pressure of gas bottle to certain value. Attention: Bottles of different gas types have different screw threads and therefore other pressure reducers
6	2 Gas bottles: 1x N ₂ (by Linde GmbH, 10l, nitrogen 5.0) 1x synth. Air (Linde GmbH, 10l)	Adjustment of different gas atmospheres/concentration inside the Raman stage

For all the experiments, following parameters have been set:

- Pressure reducer: 2 bar each
- Flow rate in flow-meter: 100l/h

3.3.2 Measurement Chamber

The measurement chamber is probably the most important part of the set-up besides the Raman spectrometer itself. After considering the requirements, the Linkam HFSX350 system was considered as suited choice. It can be attached like any other standard Raman stage to the instrument and an additional temperature control unit can heat the system locally up to 350°C. Next, it provides valves for the inflowing and outflowing gases. The sample holder, which can be locally heated, is located in the middle of the system, underneath a translucent glass window. Finally, adjustable metallic tips, which can be connected to BNC ports by soldering, can be mounted on the sample itself. A closer look on the different parts of the system is given by Figure 26 to Figure 28.

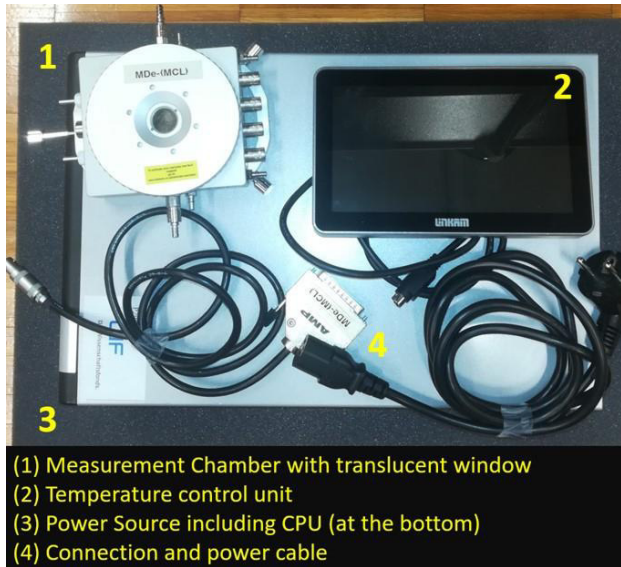


Figure 26: Linkam measurement chamber with included temperature control system

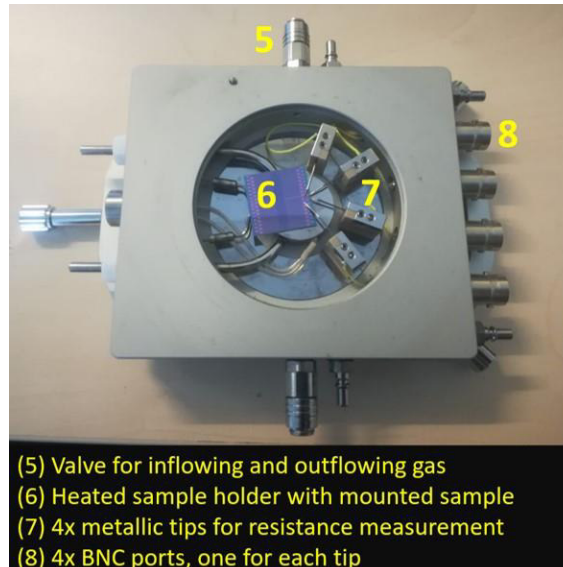


Figure 27: Mounted sample in the middle of the measurement chamber

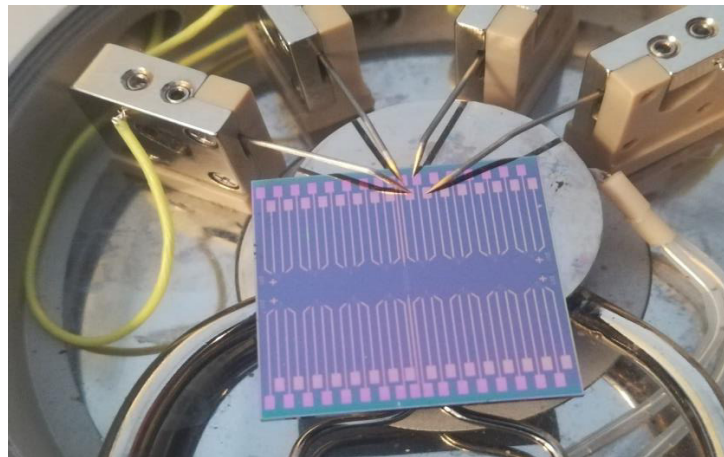


Figure 28: Close-up view of a contacted sample

The close-up shot in Figure 28 shows how one of the 16 separate gas-sensing structure of a FunkyNano platform chip is mounted and contacted. It is important to put the tips on the sample according to its design, connecting the outer electrodes and the inner electrodes of the structure with each other. To simplify the process, it is done with the chamber directly attached to the Raman spectroscopy, using the microscope for mounting the tips onto the electrodes. Before operation, all the connections and the soldering should be controlled by using a digital multimeter (e.g. Voltcraft VC170).

3.3.3 Electrical characterization

In this chapter, the equipment used for the electric resistance measurement is summarized. The author chose the 4-point resistance measurement set-up for the in-operando characterization of the samples to exclude any influence of a possible high contact resistance. A picture of the connection cables in use is seen in Figure 29, while Figure 30 shows the SMU instrument (Source Meter 2461 by Keithley) connected to provided free software kickstart (version 1.9.8.21) via a computer. The SMU unit was used in the pre-programmed 4-point resistivity measurement mode and data stored via software.



Figure 29: Different cables in use



Figure 30: The SMU connected with the provided software during measurements

Number	Name/Description	Table 8: List of used cables and connectors for the electric measurements, according to the numbering used in Figure 29.
1	4x contact test lead in black (conduction line) (Voltcraft lead, 4mm – 4mm)	
2	4x contact test lead in red (grounding line) (Voltcraft lead, 4mm – 4mm)	
3	4x BNC cable (unknown)	
4	4x BNC – 4mm connector (BKL Electronic)	

3.3.4 Raman spectrometer

All the measurements were performed on Horiba Jobin Yvon Labram300 integrated Raman system. A microscope is coupled confocally to a 300-mm focal length spectrograph which is equipped with two switchable gratings. Spectra were collected in backscattering geometry with an 1800 gr/mm grating and a charged coupled device (CCD) camera, allowing a spectral resolution of at least $1.5 \pm 0.1 \text{ cm}^{-1}$ /per pixel for the investigated range. An internal standard laser (green) of wavelength 532.02 nm was used as excitation laser. For a good use of a single spectrograph, a holographic notch filter was used for filtering the excitation line. The microscope used is a high stability BX40 from Olympus with an objective 50x with Numerical aperture (NA) of 0.55.

By using the formulas from Figure 10, we can estimate the laser spot diameter to 1.18 μm and the penetration depth to 0.8 μm . Both values could be reduced by using other objectives, however, the working distance of other available objectives did not allow to focus the laser on the surface of the sample because of the glass window, which limited the working distance. Finally, the adjustable confocal hole was set to 1000 μm and for increasing the spectral resolution, the entrance slit to 100 μm . Table 9 summarizes the used acquisition time and number of accumulations for every single measurement.

A detailed description of all the single parts and their function can be found in literature (e.g., Refs ^{46,47}).

Table 9: Acquisition time and number of accumulations for different types of measurement

Measurement	Material	Acquisition time	Number of accumulations
Phase analysis in thin film samples	ZnO	60	5
	CuO	120	5
In-operando characterization of thin films samples	ZnO	180	5
	CuO	180	5

Higher acquisition times lead to higher obtained intensities and therefore an improved signal-to-noise ratio²⁷. Nevertheless, the user should be aware of rising measurement times and a possible overexploitation of the CCD sensor (for used CCD: limit 65000 counts). The spectrum quality in terms of noise is also improved by higher number of accumulations, again leading to long measurement times²⁶.

After measurement procedure, the spectra are deconvoluted with a sum of the Gaussian-Lorentzian peak functions in a commercial software environment (Labspec 4.02, Horiba Jobin Yvon, Origin Pro 2017G). In general, spectral fitting requires a lot of experience to derive reliable information about the peak position and other characteristics of the emitted signal. Only careful fitting allows the investigator to extract both qualitative and quantitative information on the investigated material from the spectra⁴⁸.

3.3.4 Measurement procedure

The procedure for the in-operando Raman characterization is as follows:

- Mount the measurement chamber on the Raman stage
- Assembly the pressure reducer on the gas bottles according to manufacturer's instruction
- Connect gas tubes with the gas bottles, flow-meter and Raman chamber according to Figure 22. Then, set up the 4-point electric resistance measurement, leaving the gas bottles screwed down and SMU switched off
- Attach the temperature control unit to the system

- Position the sample in the middle of the measurement chamber, mount the metallic tips on the electrodes as described in chapter 3.3.3. The Raman's microscope can be used to simplify the procedure
- Close the measurement chamber, focus the Raman spectrometer on the surface of the sample with the help of the microscope and heat the sample up to 350°C by turning on the temperature control unit
- Switch on the SMU, start the provided software and measurement program. Save the measured data on the laptop
- After reaching the set temperature, wait 10 minutes until the sample has warmed through. Supply the system then with target gas by opening the gas valve
- Wait now until the system reaches equilibrium (approximately 0.5 – 1h, resistance value of the material is not changing anymore)
- Refocus the laser on the surface. Start the Raman measurement with set-up according to chapter 3.3.4
- After finishing the measurement, turn off all the instruments and let the system cool down after measurements.

Before changing the gas atmosphere, the author recommends the system to cool down, wait for thermal equilibrium (approximately 15 minutes) and to start the measurement procedure again. The reason is, that at elevated temperatures, the surface coverage for chemisorption is high and chemical bonds may not be dissolved by change of atmosphere. After cooling down to room temperature and sometime however, the chemical bonds dissolve and the surface can be covered by a new species after the atmosphere inside the chamber has changed.

4. Results and Discussion

Chapter 4 finally presents the results obtained by the experiments and discusses how the data can be interpreted. It is divided into 2 subchapters, as follows:

- Metal-oxide thin film characterization:
Light microscopy will give valuable information about the surface state and quality of produced thin films. With help of interferometric measurements, the film thickness is measured, while Raman spectroscopy unravels chemical composition and the presence of undesired phases.
- In-operando characterization of the gas-sensing thin-films by RS:
First, the functionality of the measurement design is proven and discussed. Then, a correlation between Raman data, surface state and structure of the material is made.

4.1 Metal-oxide thin film characterization

4.1.1 Light Microscopy

a) CuO:

Figure 31 shows the gas-sensing metal oxide film sprayed onto the provided substrate. Apparently, a homogeneous cupric oxide layer covers the whole sample, overlaying the platinum electrodes. Small agglomerates, spots where cupric oxide concentrates, are distributed randomly over the surface. These points appear as bright dots in the image. The appearance of such agglomerates is typical for the spray pyrolysis process of CuO at temperatures near 400°C⁴⁹. Nevertheless, a homogenous CuO thin film is deposited over the whole sample, with its thickness varying due to discussed agglomerates. Consequently, the film thickness is expected to be not constant and the standard deviation of the thickness value high.

Due to the lack of a clean room facility, contamination-free samples, according to the high standards of the semiconductor industry, could not be produced. Figure 32 shows different types of impurities and contamination found on samples. However, those impurities and surface defects are only found to a small extent.

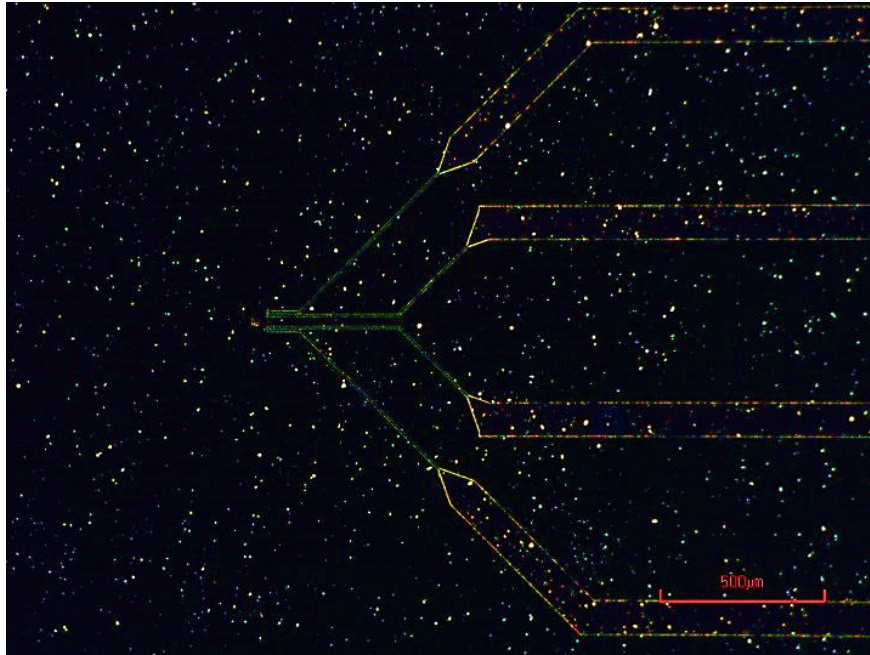


Figure 31: Cupric Oxide thin-film, seen in black, sprayed on the funky nano substrates imaged with the aid of the digital microscope in darkfield mode

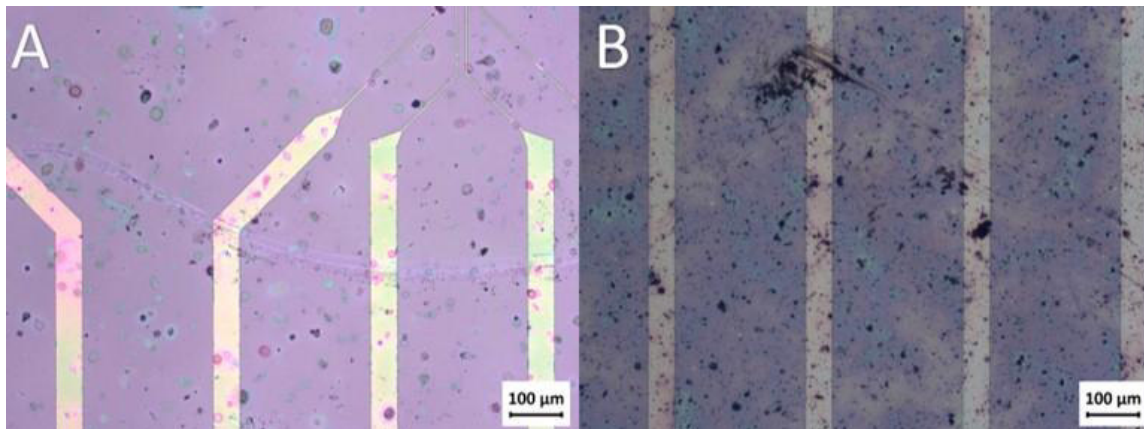


Figure 32: Some examples for found impurities or surface defects. Nevertheless, the amount of those is rather low. In (A) scratches can be seen, in (B) dirt particles are shown.

A similar situation is given in Figure 33 (a), where those bigger particles appear now as black dots in the brightfield mode of the light microscope. For structuring the CuO-film, photolithography and subsequent etching was employed. This area, see Figure 33 (b), will later be the remaining sensitive metal-oxide layer.

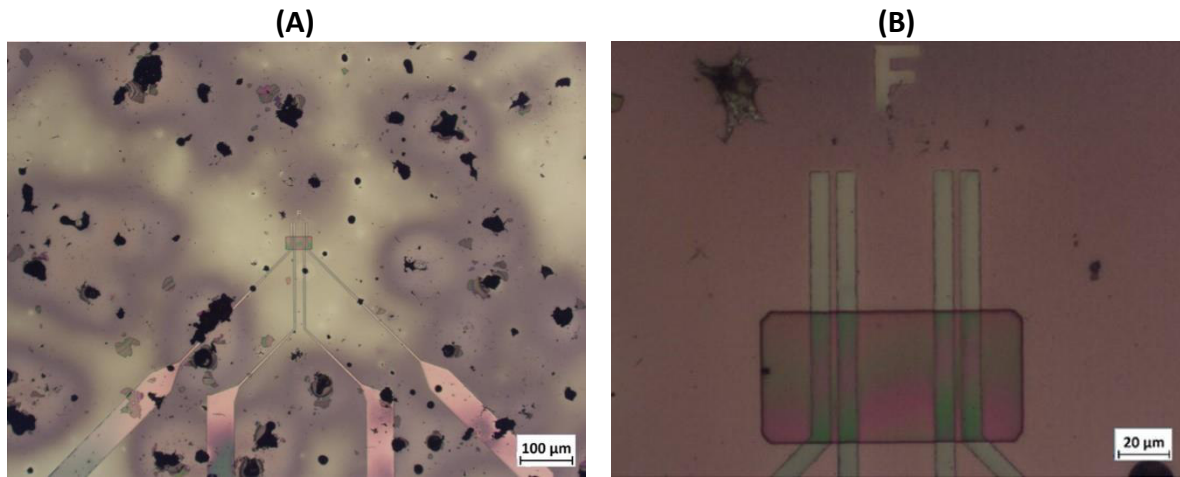


Figure 33: Surface of the CuO-sample pictured with 5x (a) and 50x (b) magnification

The result of the etching process is shown in Figure 34. Comparing Figure 34 (a) to the previous ones, most of the smaller particles are removed by etching. Nevertheless, some bigger agglomerates remain. Further etching on the contrary, to remove those particles completely, would result in the etching of areas underneath the photoresist, which should be avoided. Such a situation is shown in Figure 34(b), where the interface between MOx, photoresist and platinum electrode is slightly attacked by the etchant.

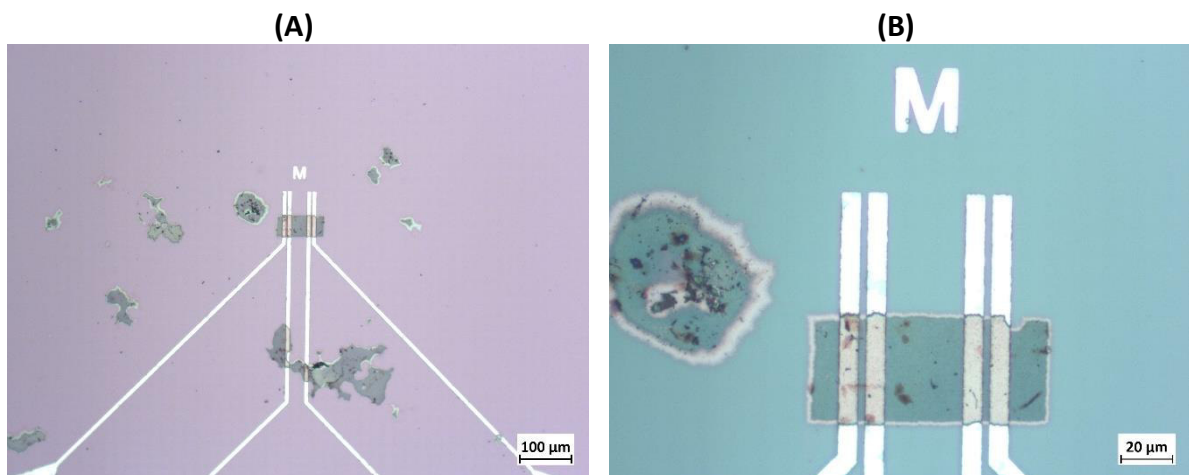


Figure 34: CuO-sample after etching. Figure 34 (a) shows the surface with 10x magnification, while in Figure 34(b) the sample is pictured with 50x magnification.

The processing of the metal-oxide thin films could be refined by adjusting some of the processing parameters. This, however, is not the purpose of this work and was done by⁴³ with a similar setup.

To sum up, a continuous metal oxide-layer of high quality, but with small impurities and inhomogeneities, was produced. Therefore, reliable Raman measurements can be performed.

b) ZnO:

The results for the ZnO are quite like the ones of CuO, as seen in both Figure 35 and 36. The lack of a clean room facility leads to a small contamination of the metal-oxide thin films. The quality of the deposited thin film is still of high quality and satisfying enough for upcoming experiments.

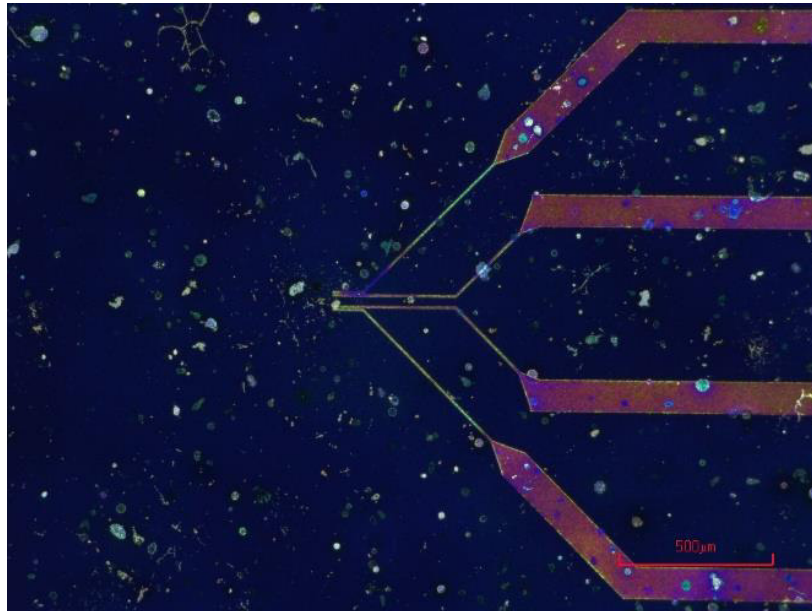


Figure 35: Zinc Oxide thin-film sprayed on the funky nano substrates imaged with the aid of the digital microscope

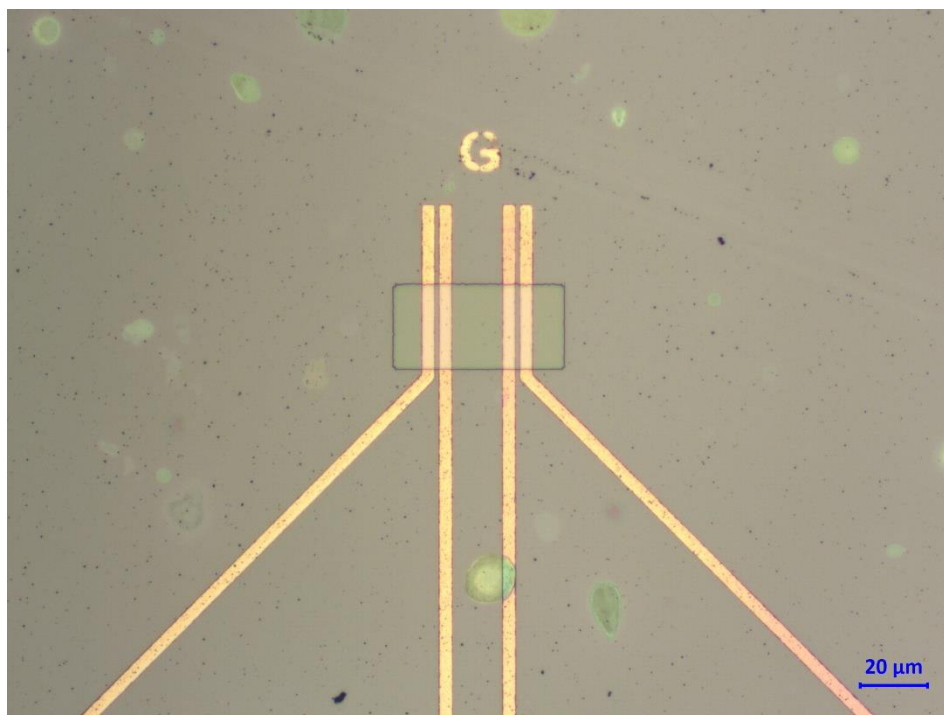


Figure 36: ZnO-sample after etching procedure with 20x magnification

4.1.2 Interferometric thickness measurement

The results of the interferometric thickness measurement are given in Table 10. It was possible to produce 155 nm thick ZnO layers on top of the FunkyNano platform chips, while the CuO layers are 220 nm thick on average. The standard deviation for the CuO samples is higher than for zinc oxide, as islands of CuO agglomerates/particles occupy the surface, see Figure 31, and therefore, the thickness values scatter more than the ones of ZnO with flatter surface.

Material	Measured thickness	<i>Table 10: Thickness measurement of both ZnO and CuO</i>
ZnO	155 nm ± 5 nm	
CuO	220 nm ± 30 nm	

4.1.3 Chemical Characterization of the thin-films by Raman

a) ZnO:

The Raman spectrum of the zinc oxide thin-films deposited on the silicon substrate is shown in Figure 37 at room temperature. At first glance, no ZnO Raman peaks can be seen, as the influence of the silicon substrate is too strong. Especially the Silicon peak near 525 cm^{-1} , see Figure 37, outnumbers all other peaks in terms of intensity. The author therefore concludes, that the signal obtained from the thin ZnO layer is very weak. Nevertheless, by looking at the Raman-shift range from 100 cm^{-1} to 500 cm^{-1} , peaks with a very low intensity can be seen (Figure 38). Comparing the 2 remaining peaks, that cannot be assigned to both SiO_2 - and Si-substrate, see Figure 15, literature^{15,39} and Figure 13, the author infers that those peaks are generated by the E_2 phonon mode of ZnO. Consequently, and with the absence of additional peaks from different phases, the deposited film is mainly of pure ZnO. To improve the gathered intensities, the author recommends concentrating on this Raman-shift range to improve the signal quality.

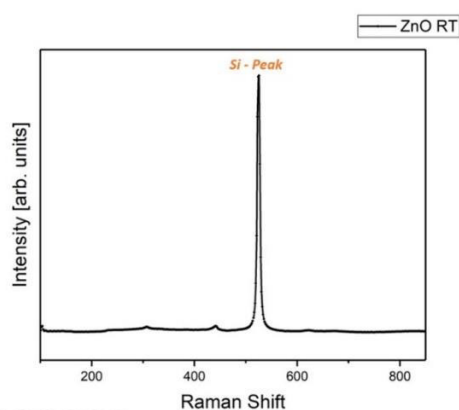


Figure 37: The Raman spectrum of ZnO, hidden under the overlaying Si- spectrum. Especially the peak at 525 cm^{-1} has strong influence on the shape of the spectrum.

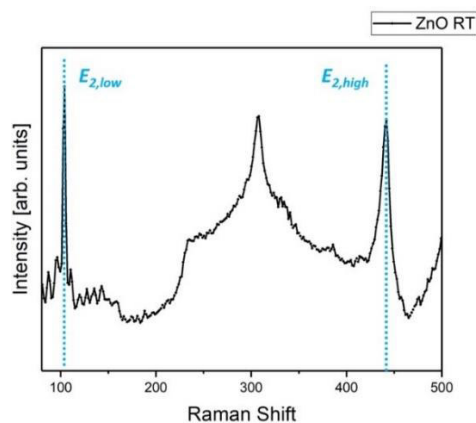


Figure 38: The Raman spectrum of the ZnO thin films deposited on the Funky nano platform chip in the range of $100 - 500\text{ cm}^{-1}$. Between 230 and 350, the second order silicon peak can be seen.

b) CuO:

The Raman spectrum of cupric oxide at room temperature is shown in Figure 39. Obviously, the influence of the substrate materials is much smaller than for ZnO. The reason for that is the higher “Raman-activity” of CuO. Thus, sharp and distinct Raman peaks, according to the predicted peaks in Figure 13 and literature⁵⁰, can be seen.

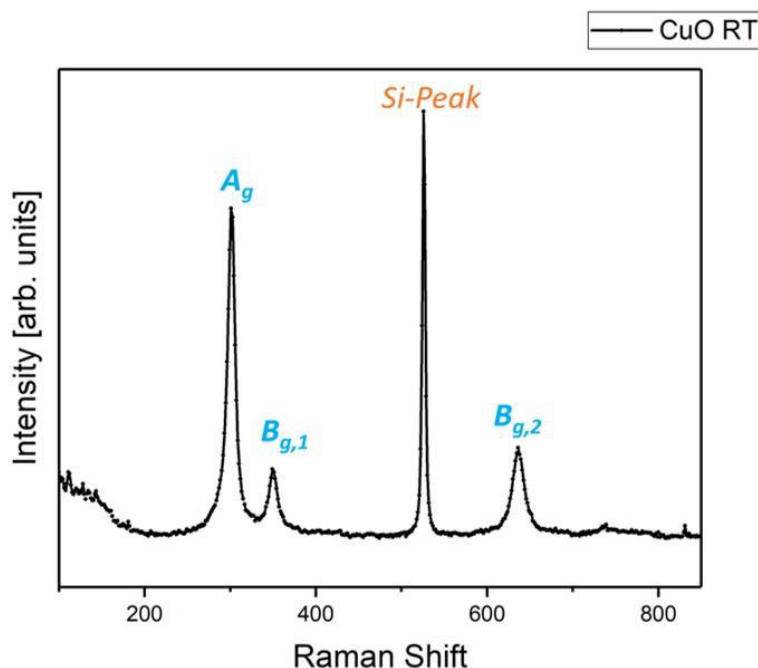


Figure 39: CuO spectrum at room temperature. Beside the strong silicon peak, the influence of the substrate and platform chip on the CuO spectrum is rather small.

4.2 In-operando Raman measurements

4.2.1 Proof of functionality – Raman measurements

In this section, the author tried to prove the functionality of the set-up in terms of Raman spectroscopy. For example, a ZnO sample was heated to 350°C under oxygen atmosphere and it was tested whether changes in the Raman spectrum can be observed. The experimental data is presented in Figure 40. First, a loss in intensity and slight shift of the peak around 440 cm^{-1} to lower wavenumbers can be determined. This effect can be related to a temperature dependent “softening” of the Raman spectra at higher temperatures⁵¹ and will be discussed in the next chapter. Additionally, the intensity of the “shoulder-peak” near 325 cm^{-1} , beside the second order silicon peak, increases its normalized intensity, shifts towards lower wavenumbers and changes its broadness. All this changes in the Raman spectra induced by the oxygen atmosphere and higher temperature, proof that the designed setup can measure structural changes in thin films during operation. A correlation between the spectra and the material is made in upcoming chapters.

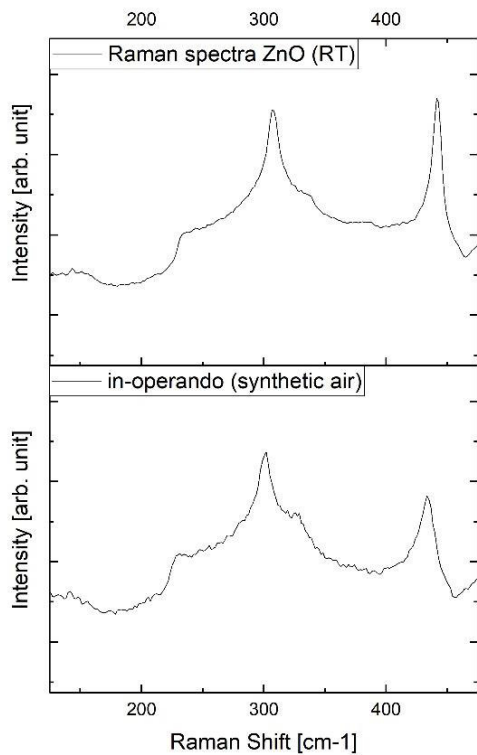


Figure 40: Change in the Raman spectrum of the deposited ZnO thin films during the operation of the sensor in synthetic air. Described solid-gas interaction induce a change in the structure of the material and therefore in its spectra

A similar experiment was done by changing the gas atmosphere additionally a second time, from synthetic air to nitrogen. This time the change in the spectra is shown using the CuO thin films in operation, see Figure 41. Again, we see a clear change in the spectra between room temperature and in operation. The difference between the O₂- and N₂ atmosphere, is only slight, as the margins are very small. This will be discussed later.

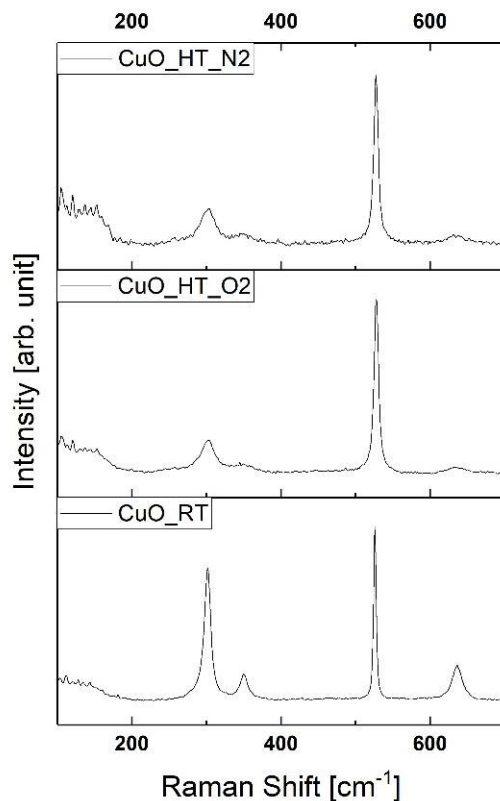


Figure 41: Change in the Raman spectrum of CuO for different sample states. At the bottom, the spectrum at room temperature is shown. In the middle, the thin film spectrum in operation at elevated temperatures in oxygen atmosphere is seen, while the top diagram presents the spectrum obtained in nitrogen atmosphere, also at elevated temperatures.

4.2.2 Correlation between Raman spectra and the gas – MOx interaction

As discussed in previous chapters, the obtained Raman spectra contain valuable information about the microstructure and the material surface – gas interactions. To analyse the spectra and extract information, following procedure must be done:

- **Determination and study of the Raman-active modes:**
Which phonon modes give rise to the spectra (see chapter 2.2.3) and which atoms are involved in the lattice vibration? In which direction do the atoms vibrate and are there any special features related to a certain mode?
- **Study of the spectrum characteristics for different circumstances:**
How do the individual features of the spectra change under different condition and how can such changes be related to microstructure or ionosorption? This step also includes the fitting and treatment of data.
- **Comparison of interpretation/conclusion with literature:**
Is the interpretation based on the obtained spectra in accordance with literature? – if not, why? How big is the influence of fitting error or other measurement uncertainties?

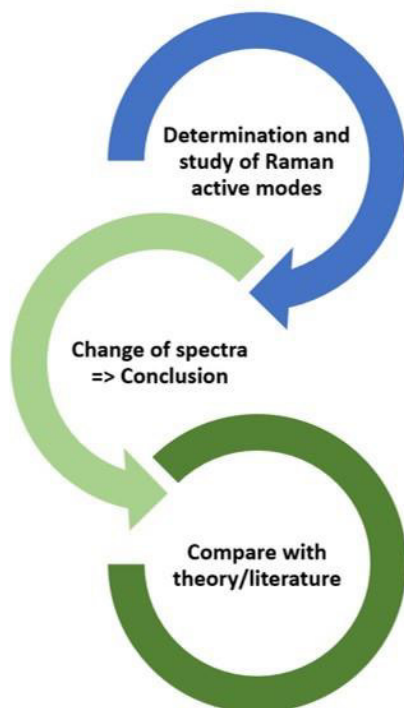


Figure 42: Summary of the correlation between Raman spectra and the interaction between MOx and gas molecules

a) CuO:

In general, there is a known and well-studied temperature influence on Raman spectra of materials. As mentioned before, this is referred to as “Raman spectrum softening”⁵². The consequence of such softening is that usually all Raman peaks lose intensity, get broader and shift towards lower peak positions⁵¹. The shifts in phonon wavenumber under variable temperature consists of two parts. The first part is caused by a volume effect, as rising temperatures lead to larger distances between atoms/molecules involved in a vibration, due to the thermal expansion. In general, this phenomenon results in the weakening of the atomic bond⁷. The second part results from the temperature dependence of the vibrational amplitudes (i.e. phonon occupation number at fixed equilibrium positions, Bose-Einstein distribution function)⁵². “Raman spectrum softening” can be seen in Figure 43, where the CuO semiconductor sample was heated to 350°C, which is usually in the range of the operation temperature of chemiresistive gas sensors, and the obtained spectra compared.

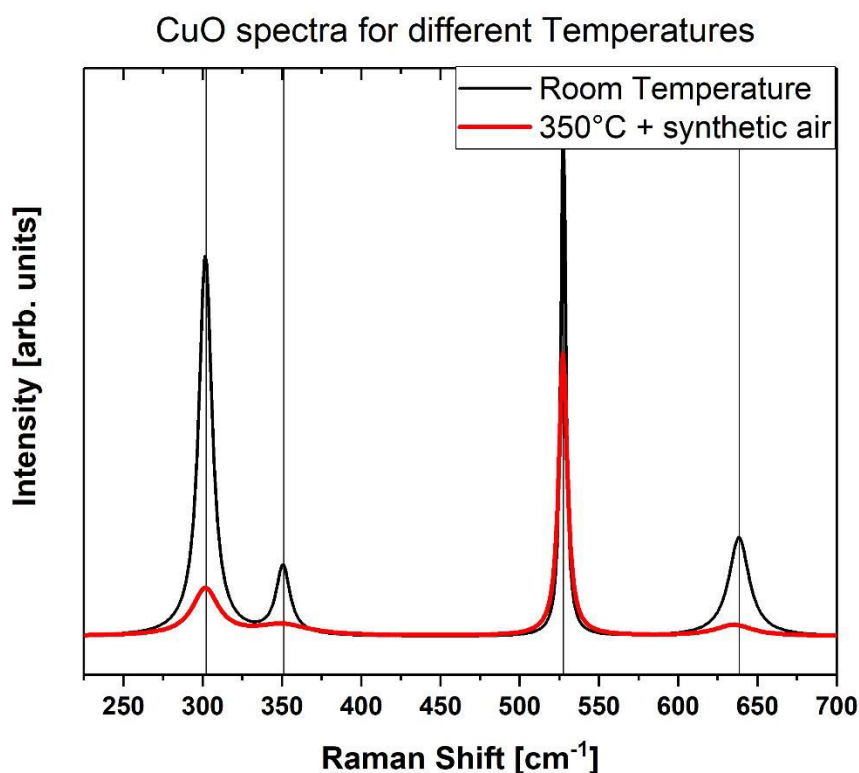


Figure 43: Change in Raman spectrum of CuO due to temperature related effects

Nevertheless, the influence of the gas – material interaction on the spectra is quite difficult to differentiate from the temperature influence, see Figure 43, as there is an overlap of both effects. To study the effects related only to the interactions happening on the surface, we must look on spectra obtained in different gas atmospheres, excluding the influence of temperature. The temperature control of the setup, provided by Linkam, is within $\pm 1^\circ\text{C}$, according to the manufacturer. A reasonable interpretation can only be done, if a temperature reference or a temperature correction is used. This can either be done by using

a Neon lamp for temperature correction, which creates a temperature independent Raman line, or by referring the Peak Position to the silicon peak at 522 cm^{-1} , which position is directly proportional to temperature⁵³. The second approach was done to correlate the spectra in different atmospheres, N_2 and synthesized air respectively, shown in Figure 44 and Table 11. For the interpretation, the A_g mode at $\sim 300\text{ cm}^{-1}$, because of its high intensity and the freestanding $B_{g,2}$ mode was used. The way the vibrational modes are vibrating inside the material are shown in the Figure 45. It can be seen, that for both modes the oxygen atoms oscillate two-dimensional around the copper atoms. Consequently, any change in the bond strength between copper and oxygen atoms, due to oxygen vacancies for example, would have an impact on the vibration and therefore on the resulting spectrum of each mode, as discussed in chapter 2.2.3. Moreover, it is expected that both peaks should be affected by the atmosphere change similarly, as both are dependent of the oxygen-species within the bond. In order to make results easier to interpret, the normalized intensity values of the modes for different atmospheres were used.

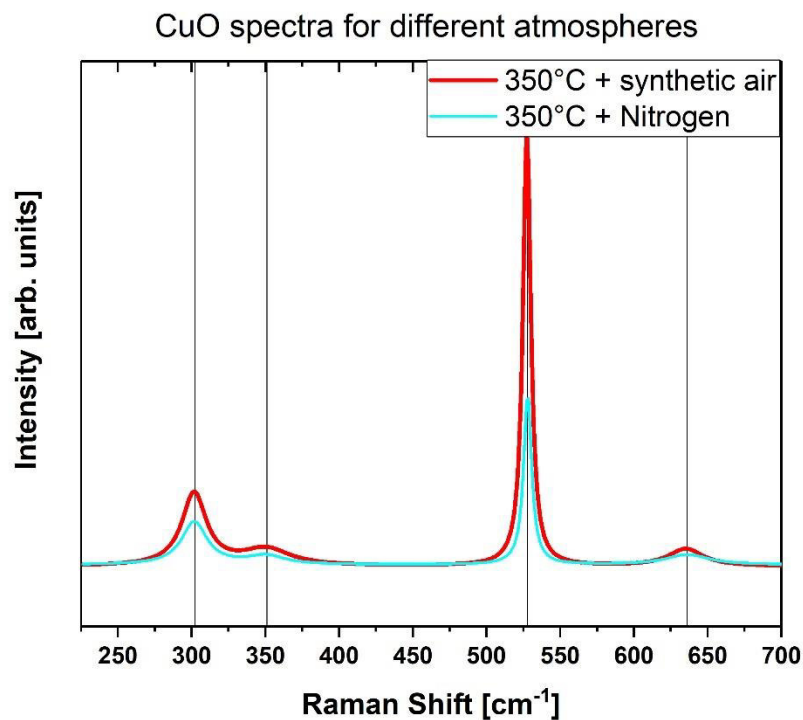


Figure 44: Normalized Raman spectrum of CuO for different atmospheres

Raman mode	$\Delta\text{position}_{\text{O}_2 \rightarrow \text{N}_2}$	$\Delta\text{width}_{\text{O}_2 \rightarrow \text{N}_2}$	Intensity $_{\text{O}_2}$ *	Intensity $_{\text{N}_2}$ *
A_g	$0,31\text{ cm}^{-1}$	-0,71	0,17	0,25
B_{g2}	$1,49\text{ cm}^{-1}$	-6,90	0,04	0,06
* normalized intensity				
<i>Table 11: Change in the parameter of the CuO spectrum due to different gas atmosphere</i>				

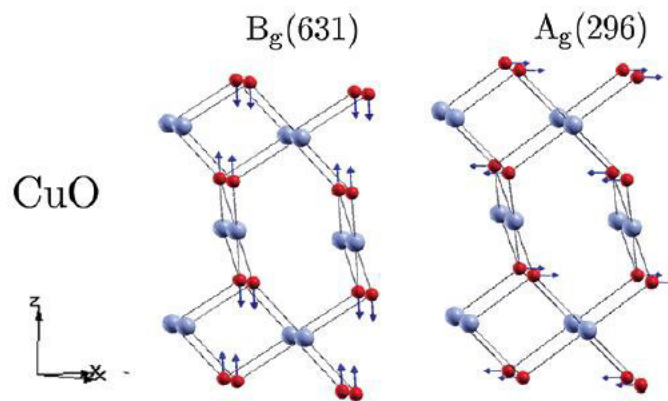


Figure 45: Raman active modes A_g and B_{g2} in the ball-and-stick model with atomic displacement shown by arrows⁵⁴. Both vibrations are one dimensional, with only the oxygen atoms (red) moving along the crystal axis c for B_{g2} and along b for A_g .

The conclusions, obtained by studying Table 11, are following:

- Change in Intensity:
There is a change towards higher normalized intensities for both peaks due to the absence of oxygen molecules in the N_2 atmosphere/on the metal-oxide surface. Normally, such a phenomenon can be related to charge transfer processes and the polarizability of the bond. This would mean, that the charge transfer mechanism for p-type semiconductor, therefore the accumulation of holes, increases the intensity compared to the silicon peaks. But we must be cautious interpreting intensity-related data obtained by the given MOx samples. As the thickness of the MOx thin-films is not constant over the whole sample, also the intensity (\approx signal coming from certain depth and therefore proportional to the thickness of the thin film) will vary. Consequently, a sound interpretation based on the intensity should be dealt with care.
- Change in the width:
A change in the width (= Full width at half maximum) can be related to a change in the coherency of the vibration. Thus, temperature related effects and the disorder will influence this spectrum parameter. By changing the atmosphere from synthetic air to nitrogen, the peaks become sharper (width decreases). This means that the disorder inside the material is decreased, while the vibrations in general become more coherent. The reason behind this phenomenon can be understood by looking at the target gas - MOx interactions. The oxygen, which is adsorbed by chemisorption, induces a charge transfer accompanied by the creation of defects⁵⁵ inside the CuO, as oxygen vacancies for example. By changing the atmosphere to N_2 , the number of adsorbed oxygen molecules decreases and consequently the number of vacancies as well. Thus, the peaks get sharper.

- Change in the peak position:

The peak position is dependent of the strength of the atomic bond. It is normally influenced by any changes in the bond distance or spring constant. For both vibration modes in study, the peak position shifts towards higher wavenumbers, if the atmosphere is changed. This means that the energy of the vibrations increases in the absence of oxygen vacancies, with the B_{g2^-} mode more affected by the absence.

To conclude, the interpretation of the spectra is in accordance with the literature. The adsorbed oxygen on the surfaces induces oxygen vacancies in the CuO thin films and results in a peak broadening and a shift towards lower Raman shifts, which can be interpreted as lower energies or weaker bonds within a vibration. Moreover, it could be shown, that the B_{g2^-} mode is more effected by this phenomenon and therefore is more sensitive. In addition to that, it appears that the normalized intensity of the studied modes is decreasing in the presence of chemisorbed oxygen molecules on the MOx surface.

b) ZnO:

The results for ZnO are comparable to the previous of CuO. As mentioned before, in chapter 4.1.3, the focus lies on the peak of the mode positioned at $\sim 450\text{cm}^{-1}$ ($E_{2,\text{high}}$). The change in the peak position, intensity and broadness is shown in Figure 46. Again, the absence of oxygen on the MOx surface induces a shift towards higher energies, or higher Raman shifts respectively, for the same reasons as for CuO. Moreover, the fitting of the data confirms that the width of the peak decreases in nitrogen atmosphere, as seen in table 12. Consequently, the same conclusion as for CuO can be drawn.

However, it is very interesting that the normalized intensity of the $E_{2,\text{high}}$ mode decreases in the absence of adsorbed oxygen on the surface, exactly to the opposite of the p-type conductor CuO, with ZnO being a n-type semiconductor. This is can be seen in Figure 46 and in Table 12. At this point, it should be mentioned that the normalized intensities of the ZnO sample is much higher as the one of CuO, as the $E_{2,\text{high}}$ -peak was normalized with the second order silicon peak and not the one at $\approx 522\text{ cm}^{-1}$ as in CuO. Still, the information extracted from the peak intensities must be treated with care, as the film thickness is not constant over the sample and might have an additional influence. Further investigations on films with constant thickness or simulations would give clarity.

Raman mode	$\Delta\text{position}_{\text{O}_2 \rightarrow \text{N}_2}$	$\Delta\text{width}_{\text{O}_2 \rightarrow \text{N}_2}$	Intensity $_{\text{O}_2}$ *	Intensity $_{\text{N}_2}$ *
$E_{2,\text{high}}$	$0,48\text{ cm}^{-1}$	-1,74	0,83	0,64
* normalized intensity				
<i>Table 12: Change in the parameter of the ZnO spectrum due to different gas atmosphere</i>				

ZnO Raman spectra for different atmospheres

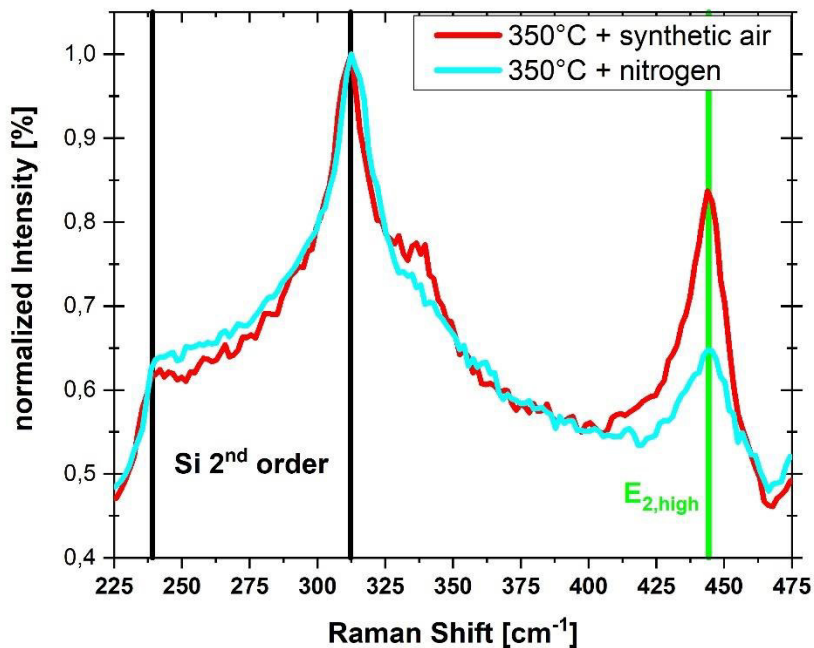


Figure 46: Normalized Intensities for ZnO in different gas atmospheres

c) General conclusion:

In general, we can conclude, that for both metal-oxide semiconductors the results and the interpretation of the Raman spectra is in accordance with the gas - MO_x surface interaction mechanism provided by Ionosorption¹³ and Oxygen vacancy⁵⁵ theory. Therefore, it was proven that the measurement set-up can detect surface related phenomena and that Raman spectroscopy is well suited for an in-operando characterization of gas-sensing MO_x thin films and their devices.

Nevertheless, the signal-to-noise ratio for all metal-oxide thin film samples was quite low. A high surface roughness due to the processing combined with the signal coming from a small sample volume is the reason for the low signal intensities. Although the signals achieved from the comparatively thin MO_x layer are lower than from bulk samples, the data can be unambiguously interpreted. This demonstrates that Raman spectroscopy is a highly useful tool for studying thin films, which are used specifically for chemical sensors.

5 Summary and Outlook

Within this thesis, gas sensitive metal-oxide thin films, CuO and ZnO respectively, were produced by spray pyrolysis technique. The pure films were deposited on a specific silicon-based platform chip and processed to gas-sensing samples, using photolithography and subsequent etching. Moreover, an in-operando system was designed and setup, which enables studying structural changes of gas sensing materials in various gaseous atmospheres by Raman spectroscopy, and simultaneous electrical characterization. Finally, the functionality of the system was proofed and an introduction into spectra correlation was given.

Studying gas-sensing materials by means of Raman spectroscopy has proven to be a very powerful approach, as the obtained data could be very well correlated to the interactions between target gases and the surface of the metal oxide materials, which are in accordance with recent studies and theory. The author proved, that the presence of oxygen on the surface introduces a shift in the Raman peak position towards lower wavenumbers and leads to peak-broadening. Moreover, it has been shown, that adsorbed gases have a different impact on the spectra intensities, depending on the type of semiconducting metal-oxide material.

Although the setup has been designed and set up for simultaneous electrical measurements of the metal oxide layers, it is not feasible to characterize the electrical resistance, with the given set-up. This was due to the employed tip-system which has only limited possibilities for contacting the Ti-Pt pads on the silicon-based platform chips. An improved setup or the use of wire bonding for contacting the sensor system will be used in the future to enable simultaneous electrical and optical measurements.

For future work, an updated system is a powerful and flexible tool for investigating a variety of physical and chemical questions:

- Studying surface-gas interactions for various gas-material combinations, where the reaction mechanisms are not yet clear – for example in presence of metal nanoparticles changing the band structure of the gas sensing material.
- 2D-mapping of the sample and detection of temperature profiles along a gas sensitive layer integrated on micro-hotplates.
- Measurement of doping profiles.
- Measurement of electrical conductivity and correlation with structural changes induced by target gases.

Further upgrading the system with a UV excitation laser and UV-capable spectrometer to enable additional photoluminescence spectroscopy. By using this technique, processes directly related to the change in energy band structure can be studied. The use of a UV laser source (lower wavelength as present system) would decrease the penetration depth and an overlap of the different Raman spectra could be avoided. This could result in a higher resolution in terms of signal-noise ratio and in improved calculations based on simulations.

6. List of Figures

Figure 1: Working principle of a gas sensor device	7
Figure 2: Schematic of a chemiresistive gas sensor.....	8
Figure 3: The different interaction mechanism between a gas and a solid.....	9
Figure 4: Lennard-Jones model for physisorption and chemisorption.....	10
Figure 5: Density of adsorbed gas molecules as function of temperature.....	11
Figure 6: Bending of the energy band due to Ionosorption	12
Figure 7: Hexagonal wurtzite-type lattice.....	13
Figure 8: The unit cell of the complex monoclinic lattice	14
Figure 9: Schematics and formula for the lateral (A) and axial (B) resolution.....	15
Figure 10: The Raman effect.....	17
Figure 11: Features of a Raman spectrum	18
Figure 12: Raman spectrum of CuO	19
Figure 13: Raman spectrum of ZnO	20
Figure 14: Raman spectra of ZnO thin films on a (0 0 1)-Si substrate	21
Figure 15: Raman spectra of silicon	21
Figure 16: Workflow towards the in-operando characterization of MOx thin films	22
Figure 17: FunkyNano platform chip	22
Figure 18: Spray pyrolysis set-up at MCL Forschungs GmbH.....	23
Figure 19: Photolithography	25
Figure 20: Process scheme of the photolithography process.....	25
Figure 21: CuO thin film on SiO ₂ reference platelet.....	28
Figure 22: A schematic sketch of the overall measurement setup	29
Figure 23: The in-operando gas sensing metal-oxide characterization setup.....	30
Figure 24: Different parts of the gas supply system	30
Figure 25: Nitrogen and synthetic air gas bottles.....	30
Figure 26: Linkam measurement chamber	32
Figure 27: Mounted sample in the middle of the measurement chamber	32
Figure 28: Close-up view of a contacted sample	32
Figure 29: Different cables in use	33
Figure 30: The SMU connected with the provided software during measurements	33
Figure 31: Cupric Oxide thin-filme	37
Figure 32: Some examples for found impurities or surface defects.....	37
Figure 33: Surface of the CuO-sample	38
Figure 34: CuO-sample after etching	38
Figure 35: Zinc Oxide thin-film sprayed on the funky nano substrates.....	39
Figure 36: ZnO-sample after etching procedure.....	39
Figure 37: The Raman spectrum of ZnO	40
Figure 38: The Raman spectrum of the ZnO thin films deposited on the Funky nano platform chip in the range of 100 – 500 cm ⁻¹	40
Figure 39: CuO spectrum at room temperature	41
Figure 40: Change in the Raman spectrum of the deposited ZnO thin films during the operation	42
Figure 41: Change in the Raman spectrum of CuO for different sample states.....	42
Figure 42: Summary of the spectra – interaction correlation	43
Figure 43: Change in Raman spectrum of CuO due to temperature related effects.....	44
Figure 44: Normalized Raman spectrum of CuO for different atmospheres.....	45
Figure 45: Phonon modes of CuO	46
Figure 46: Normalized Intensities for ZnO in different gas atmospheres.....	48

8. List of Tables

Table 1: Advantages and Disadvantages of semiconductor MO _x -based gas sensor devices	8
Table 2: Properties of ZnO	13
Table 3: Properties of CuO	14
Table 4: Different equipment parts for spray pyrolysis set-up listed	24
Table 5: Spray Pyrolysis process parameters for the different materials (ZnO, CuO)	24
Table 6: Photolithography set-up	26
Table 7: Equipment listed for the gas supply system	31
Table 8: List of used cables and connectors	33
Table 9: Acquisition time and number of accumulations for different types of measurement.....	34
Table 10: Thickness measurement of both ZnO and CuO	40
Table 11: Change in the parameter of the CuO spectrum due to different gas atmosphere	45
Table 12: Change in the parameter of the ZnO spectrum due to different gas atmosphere.....	47

9. References

1. Mutinati, G. C. 3D-CMOS integrable gas sensor device based on nanocrystalline tin dioxide films. (2013).
2. Korotcenkov, G. *Chemical Sensors: Simulation and Modeling Vol 2: Conductometric-Type Sensors*. *Chemical Sensors: Simulation and Modeling Vol 2: Conductometric-Type Sensors* (Momentum Press, 2012). doi:10.5643/9781606503140
3. S, S. Gas Sensing Properties of Metal Oxide Nanowires and their CMOS Integration. 1–171 (2014).
4. Brunet, E. Fabrication of tin oxide nanowire gas sensors. (2014).
5. Hummel, R. E. *Electronic Properties of Materials*. (Springer New York, 2011). doi:10.1007/978-1-4419-8164-6
6. Lalauze, R. *Physical Chemistry of Solid-Gas Interfaces*. *Physical Chemistry of Solid-Gas Interfaces* (ISTE, 2008). doi:10.1002/9780470611296
7. Ashcroft, N. W. & Mermin, N. D. *Solid State Physics*. (Holt, Rinehart and Winston, 1976).
8. Atkins, P., de Paula, J. & Keeler, J. *Atkins' physical chemistry*. (Oxford university press, 2018).
9. Madou, M. J. & Morrison, S. R. *Chemical sensing with solid state devices*. (Elsevier, 2012).
10. Mortimer, C. E. & Müller, U. *Chemie: das Basiswissen der Chemie; 126 Tabellen*. (Georg Thieme Verlag, 2007).
11. Batzill, M. & Diebold, U. The surface and materials science of tin oxide. *Progress in surface science* **79**, 47–154 (2005).
12. Barsan, N. & Weimar, U. Conduction model of metal oxide gas sensors. *Journal of Electroceramics* **7**, 143–167 (2001).
13. Henrich, V. E. & Cox, P. A. *The surface science of metal oxides*. (Cambridge university press, 1996).
14. Fox, M. & Bertsch, G. F. Optical Properties of Solids. *American Journal of Physics* **70**, 1269–1270 (2002).
15. Klingshirn, C. ZnO: Material, Physics and Applications. *ChemPhysChem* **8**, 782–803 (2007).
16. Xu, J., Pan, Q. & Tian, Z. Grain size control and gas sensing properties of ZnO gas sensor. *Sensors and Actuators B: Chemical* **66**, 277–279 (2000).
17. Klingshirn, C. F., Waag, A., Hoffmann, A. & Geurts, J. *Zinc oxide: from fundamental properties towards novel applications*. **120**, (Springer Science & Business Media, 2010).
18. Marabelli, F., Parravicini, G. B. & Salghetti-Drioli, F. Optical gap of CuO. *Physical Review B* **52**, 1433–1436 (1995).
19. Samarasekera, P., Kumara, N. & Yapa, N. U. S. Sputtered copper oxide (CuO) thin films for gas sensor devices. *Journal of Physics: Condensed Matter* **18**, 2417 (2006).
20. CuO Crystal Structure: Datasheet from "PAULING FILE Multinaries Edition -- 2012" in SpringerMaterials (https://materials.springer.com/isp/crystallographic/docs/sd_0542121).

21. Guha, S., Peebles, D. & Wieting, T. J. Zone-center ($q = 0$) optical phonons in CuO studied by Raman and infrared spectroscopy. *Physical Review B* **43**, 13092–13101 (1991).
22. Weast, R. C., Astle, M. J. & Beyer, W. H. *CRC handbook of chemistry and physics*. **69**, (CRC press Boca Raton, FL, 1988).
23. Singh, I. & Bedi, R. K. Studies and correlation among the structural, electrical and gas response properties of aerosol spray deposited self assembled nanocrystalline CuO. *Applied Surface Science* **257**, 7592–7599 (2011).
24. Efremov, E. v., Ariese, F. & Gooijer, C. Achievements in resonance Raman spectroscopy. Review of a technique with a distinct analytical chemistry potential. *Analytica Chimica Acta* **606**, 119–134 (2008).
25. Cantarero, A. Raman Scattering Applied to Materials Science. *Procedia Materials Science* **9**, 113–122 (2015).
26. Graves, P. & Gardiner, D. Practical raman spectroscopy. *Springer* (1989).
27. McCreery, R. L. *Raman Spectroscopy for Chemical Analysis*. (John Wiley & Sons, Inc., 2000). doi:10.1002/0471721646
28. Rumyantseva, M. N., Gaskov, A. M., Rosman, N., Pagnier, T. & Morante, J. R. Raman surface vibration modes in nanocrystalline SnO₂: correlation with gas sensor performances. *Chemistry of materials* **17**, 893–901 (2005).
29. Gurlo, A. & Riedel, R. In situ and operando spectroscopy for assessing mechanisms of gas sensing. *Angewandte Chemie - International Edition* **46**, 3826–3848 (2007).
30. Hess, C. & Lunsford, J. H. Mechanism for NO₂ storage in barium oxide supported on magnesium oxide studied by in situ Raman spectroscopy. *The Journal of Physical Chemistry B* **106**, 6358–6360 (2002).
31. Long, D. A. & Long, D. A. *Raman spectroscopy*. **276**, (McGraw-Hill New York, 1977).
32. Lewis, I. R. & Edwards, H. *Handbook of Raman spectroscopy: from the research laboratory to the process line*. (CRC Press, 2001).
33. Amer, M. *Raman spectroscopy for soft matter applications*. (John Wiley & Sons, 2009).
34. Gouadec, G. & Colomban, P. Raman Spectroscopy of nanomaterials: How spectra relate to disorder, particle size and mechanical properties. *Progress in crystal growth and characterization of materials* **53**, 1–56 (2007).
35. Harris, D. C. & Bertolucci, M. D. *Symmetry and spectroscopy: an introduction to vibrational and electronic spectroscopy*. (Courier Corporation, 1989).
36. Kroumova, E. *et al.* Bilbao crystallographic server: useful databases and tools for phase-transition studies. *Phase Transitions: A Multinational Journal* **76**, 155–170 (2003).
37. Chrzanowski, J. & Irwin, J. C. Raman scattering from cupric oxide. *Solid state communications* **70**, 11–14 (1989).
38. Özgür, Ü. *et al.* A comprehensive review of ZnO materials and devices. *Journal of applied physics* **98**, 11 (2005).
39. Xu, X. L., Lau, S. P., Chen, J. S., Chen, G. Y. & Tay, B. K. Polycrystalline ZnO thin films on Si (1 0 0) deposited by filtered cathodic vacuum arc. *Journal of Crystal Growth* **223**, 201–205 (2001).

40. Borowicz, P. *et al.* Deep-ultraviolet Raman investigation of silicon oxide: Thin film on silicon substrate versus bulk material. *ADVANCES IN NATURAL SCIENCES: NANOSCIENCE AND NANOTECHNOLOGY* **3**, 45003–45007 (2012).
41. Perednis, D. & Gauckler, L. J. Thin film deposition using spray pyrolysis. *Journal of electroceramics* **14**, 103–111 (2005).
42. Andrade, E. & Miki-Yoshida, M. Growth, structure and optical characterization of high quality ZnO thin films obtained by spray pyrolysis. *Thin Solid Films* **350**, 192–202 (1999).
43. Radl, L. Fabrication of Copper Oxide Thin Films by Spray Pyrolysis Technique for CMOS Integrated Conductometric Gas Sensors. (2019).
44. Mack, C. *Fundamental principles of optical lithography: the science of microfabrication*. (John Wiley & Sons, 2008).
45. Prasankumar, R. P. & Taylor, A. J. *Optical techniques for solid-state materials characterization*. (CRC Press, 2016).
46. Smith, E. & Dent, G. *Modern Raman spectroscopy: a practical approach*. (Wiley, 2019).
47. Vandenabeele, P. *Practical Raman spectroscopy: an introduction*. (Wiley Online Library, 2013).
48. Yuan, X. & Mayanovic, R. A. An empirical study on Raman peak fitting and its application to Raman quantitative research. *Applied spectroscopy* **71**, 2325–2338 (2017).
49. Oh, S. W., Bang, H. J., Bae, Y. C. & Sun, Y.-K. Effect of calcination temperature on morphology, crystallinity and electrochemical properties of nano-crystalline metal oxides (Co₃O₄, CuO, and NiO) prepared via ultrasonic spray pyrolysis. *Journal of Power Sources* **173**, 502–509 (2007).
50. Chrzanowski, J. & Irwin, J. C. Raman scattering from cupric oxide. *Solid State Communications* **70**, 11–14 (1989).
51. Cuscó, R. *et al.* Temperature dependence of Raman scattering in ZnO. *Physical Review B* **75**, 165202 (2007).
52. Xu, J. F. *et al.* Raman spectra of CuO nanocrystals. *Journal of Raman spectroscopy* **30**, 413–415 (1999).
53. Deluca, M. *et al.* In-Situ Temperature Measurement on CMOS Integrated Micro-Hotplates for Gas Sensing Devices. *Sensors* **19**, 672 (2019).
54. Debbichi, L., Marco De Lucas, M. C., Pierson, J. F. & Krüger, P. Vibrational properties of CuO and Cu₄O₃ from first-principles calculations, and raman and infrared spectroscopy. *Journal of Physical Chemistry C* **116**, 10232–10237 (2012).
55. Carpenter, M. A., Mathur, S. & Kolmakov, A. *Metal oxide nanomaterials for chemical sensors*. (Springer Science & Business Media, 2012).
56. Deluca, M. Vorlesungsskriptum - Moderne optische Methoden der Werkstoffcharakterisierung, Montanuniversität Leoben. in (2017).
57. Dolai, S. *et al.* Cupric oxide (CuO) thin films prepared by reactive dc magnetron sputtering technique for photovoltaic application. *Journal of Alloys and Compounds* **724**, 456–464 (2017).